Defence Research and Development Canada

Recherche et développement pour la défense Canada

DEFENCE R&D DÉFENSE

Adaptive optics system for remote sensing applications of filamentation

Jean-François Daigle and Robert Bernier

Prepared by:
Les instruments optiques du Saint-Laurent inc.
5 rue de Grandpré
Boucherville, (Québec)
J4B 4Z6

Project Manager: Robert Bernier 450-641-3624
Contract Number: W7701-071506
Contract Scientific Authority: Gilles Roy, 418-844-4000 (4335)

Defence R&D Canada – Valcartier

Canada

Adaptive optics system for remote sensing applications of filamentation

Jean-François Daigle and Robert Bernier

Prepared by:
Les instruments optiques du Saint-Laurent inc.
5 rue de Grandpré
Boucherville, (Québec)
J4B 4Z6

Project Manager: Robert Bernier 450-641-3624

Contract Number: W7701-071506

Contract Scientific Authority: Gilles Roy, 418-844-4000 (4335)

Defence R&D Canada – Valcartier

Principal Author

Original signed by Jean-François Daigle

....

Jean-François Daigle

Approved by

Original signed by Gilles Roy

....

Gilles Roy

Defence scientist

Work performed under: TIF: 10DC05: Powerful femtosecond laser pulses in the far IR for standoff Chem-Bio detection

Abstract

Laser filaments represent a potentially useful tool in terms of remote and atmospheric applications. Indeed, the high intensity inside the filament core induces nonlinear effects which can broaden the spectrum from the ultraviolet to the mid-infrared. This white light laser could be used as an effective counter measure to blind detectors or guide missiles away from the target. Moreover, its intensity is sufficiently high to ionize the transparent medium in which it propagates. The ionized atoms and molecules recombine and emit a fingerprint fluorescence, characteristic of the ionized elements. This property of filamentation opens the way for remote sensing applications. However, the generation and control of those filaments poses real challenges. This report is about the work that has been done at RDDC-Valcartier, in collaboartion with Laval University, to design, develop and test an adaptive optics (AO) system to be used with a lidar in remote sensing applications. This AO system has been tested to allow initiation of filaments as far as 120 m from the lidar laser source. Also, in this work, the influence of atmospheric turbulences on the initiation and strength of the filamentation process has been studied.

Résumé

Des filaments laser représentent un outil utile pour les applications en télédétection et études atmosphériques. Les grandes intensités réalisées au coeur des filaments induisent des effets non-linéaires qui élargissent le spectre lumineux de l'ultraviolet jusqu'au moyen infrarouge. Cette lumière blanche pourrait être utilisée à titre de contre-mesure aux fins d'aveugler des détecteurs ou pour dévier des missiles de leur cible. De plus, leur intensité est suffisamment élevée pour ioniser le milieu transparent dans lequel ils se propagent. Les atomes et molécules ainsi ionisés se recombinent en émettant une fluorescence dont la signature est caractéristique des éléments ionisés. Cette propriété des filaments laser conduit à diverses applications en télédétection. Cependant, la génération et le contrôle de ces filaments posent de sérieux défis. Ce rapport concerne les travaux menés au RDDC-Valcartier, en collaboration avec l'Université Laval, dans le but de concevoir, développer et tester un système d'optique adaptative (OA) pouvant être utilisé avec un lidar dans des applications de télédétection. Lors de tests, ce système OA a permis le contrôle du début de la filamentation à une distance aussi grande que 120 m du lidar. Aussi, dans ce travail, l'influence des turbulences atmosphériques sur le processus d'initiation et sur l'intensité des filaments a été étudiée.

This page intentionally left blank.

Executive summary

Adaptive optics system for remote sensing applications of filamentation

Jean-François Daigle; Robert Bernier; DRDC Valcartier CR 2011-539; Defence R&D Canada – Valcartier; March 2011.

Introduction or background:

When propagating in the atmosphere, the non-linear behavior of intense ultrashort laser pulses leads to the formation of long plasma channels or filaments with unique properties. They represent a potential breakthrough towards the development of atmospheric tools in the field of LIDAR remote sensing.

However, the formation of filaments suitable for atmospheric studies at long distance remains an issue. In this document, we report the results of the work that has been done at RDDC-Valcartier and Laval University to develop and test an Adaptive Optics (AO) system to control the filamentation process. The effects of the atmospheric turbulences on the plasma channels are also investigated.

Results:

The AO system has been designed, developed and tested. It was experimentally demonstrated that the AO system can be used to efficiently deliver focused laser pulses and initiate filamentation at distances as large as 120 m, which is in itself a most promising accomplishment.

The capability of the lidar with AO system for remote sensing applications was confirmed by detecting fluorescence from the N_2 species at the distance of 120 m. The fluorescence from the N_2 species is the result of multiphoton ionization attributed to the high intensity inside the filament core.

Significance:

Remote detection and identification of the spatial distribution of atmospheric pollutants like NO_x, SO_2, O_3, Hg, Benzene, Toluene, methane or other Volatile Organic Compounds (VOC) could be rendered feasible with laser filamentation. In addition, this *white light* laser could be used as an effective counter measure to blind detectors or guide missiles away from their target.

Future plans:

Future research will try to verify whether the lidar signal itself from the N_2 species could be a better signal for monitoring and controlling the quality of the filamentation process.

Sommaire

Adaptive optics system for remote sensing applications of filamentation

Jean-François Daigle; Robert Bernier; DRDC Valcartier CR 2011-539; R & D pour la défense Canada – Valcartier; Mars 2011.

Introduction ou contexte:

Le comportement non-linéaire dans l'atmosphère d'impulsions laser ultra-brèves et intenses résulte en la formation de plasmas en forme de longs filaments. Les propriétés uniques de ces filaments amènent la possibilité d'une avancée majeure dans le développement des applications du lidar en télédétection.

Cependant, la formation de filaments utilisables en études atmosphériques à de longues distances demeure un défi. Dans le présent document, nous faisons rapport des résultats du travail produit au RDDC-Valcartier et à l'Université Laval pour développer et tester un système d'Optique Adaptative (OA) devant servir à contrôler le processus de filamentation. Les effets des turbulences atmosphériques sur les filaments ont aussi été étudiés.

Résultats:

Le système OA a été conçu, développé et testé. Démonstration expérimentale a été faite qu'on peut l'utiliser pour focaliser les impulsions laser et causer la formation de filaments à aussi loin que 120 m. Ce résultat est en lui-même des plus encourageants.

La capacité du lidar équipé du système OA pour les applications de télédétection a été confirmée par la détection de la fluorescence du N_2 à la distance de 120 m. La fluorescence du N_2 résulte d'un processus d'ionisation à photons multiples causé par la haute intensité dans le filament.

Importance:

La détection à distance et la mesure du profil spatial de polluants atmosphériques tels que NO_x, SO_2, O_3, Hg, Benzène, Toluène, méthane ou autres Composés Organiques Volatiles (COV) pourrait devenir possible au moyen d'un lidar à filamentation laser. De plus, cette lumière blanche pourrait être utilisée à titre de contre-mesure soit pour aveugler des détecteurs ou soit encore pour dévier des missiles de leur course.

Perspectives:

Dans un futur rapproché, la recherche tentera de montrer si le signal de fluorescence du N_2 lui-même pourrait être avantageusement mis à profit pour suivre et contrôler la qualité du processus de filamentation.

Table of contents

List of figures

Acknowledgements

This page intentionally left blank.

1 INTRODUCTION

When propagating in the atmosphere, the non-linear behavior of intense ultrashort laser pulses leads to the formation of long plasma channels with unique properties. Their discovery [1,2] awoke the interest of many researchers in the field of non-linear optics to pursue atmospheric studies using these structures nowadays called filaments [3,4,5,6]. They represent a potential breakthrough towards the development of atmospheric tools in the fields of LIDAR remote sensing [7,8,9] and electric discharge triggering/guiding [10,11] for instance.

In the specific field of Lidar remote sensing, it has been claimed that a lidar equipped with a spectrometer, analyzing the light backscattered by molecules excited by light filaments, via multiphoton ionization, could allow the remote sensing of many types of atmospheric pollutants. Several laser based methods, including remote nanosecond laser induced breakdown spectroscopy (ns-LIBS) and differential absorption LIDAR (DiAL) [12],were proposed to fulfill the requested task. However, numerous drawbacks limited the efficiency of these detection techniques. As an example, ns-LIBS provided the possibility to simultaneously identify multiple components present in a target but linear diffraction limitations at the focal spot annihilated any hopes for remote applications at reasonable laser cost and energy. On the other hand, because of its high sensitivity, DiAL proved to be very effective for long distance detection but, because it is highly selective, multiple or highly tunable laser sources would have been required to identify distinct constituents simultaneously.

On the other hand high intensity inside the filament core provides simultaneous detection of multiple components present in the target [13,14]. Moreover, due to the non-linear behavior of the laser pulse during atmospheric propagation, the technique is less affected by the diffraction limitation. In fact, filaments have been observed over several hundreds of meters from the laser source [27].

Among those contaminants, we could find such molecules or compounds as NO_x, SO_2, O_3, Hg, Benzene, Toluene, methane or other Volatile Organic Compounds (VOC) [7,8,15]. A review of the situation in the field has been presented in [16].

In the atmosphere, the filaments appear as a dynamic equilibrium between Kerr self-focusing and self-defocusing by the self-generated low-density plasma produced by multiphoton/tunnel ionization of the air molecules [2]. Indeed, for a non-uniform intensity distribution laser pulse (Gaussian, for example) with peak power higher than the critical power for self-focusing, the Kerr effect will act as a non-linear lens that will focus the light pulse until its intensity is sufficiently high to ionize the medium in which it propagates. Once the plasma is sufficiently dense to counteract the Kerr lens effect, the laser pulse will start to defocus. The defocusing nature of the plasma limits and stabilizes the light intensity in each of the filaments. In air, the clamped intensity, for laser pulses at 800 nm, is approximately 5×10^{13} W/cm^2 [17,18]. Filamentation intensity clamping represents an incredible advantage for atmospheric studies.

There are, however, at least two problems to overcome for filaments to be of practical use in remote applications. First, there needs to be found a means to control the distance at which the onset of the filamentation process will occur. Second, it has been shown that the presence of atmospheric turbulences along the propagation path of the laser source could be such as to even prevent the filamentation process from occurring [19].

In this report, an approach using Adaptive Optics (AO) is proposed in order to address the problem of controlling the onset of the filamentation process (Section 2). Further, some experimental results are presented showing that the detection of atmospheric pollutants is indeed possible with such a lidar instrument equipped with the AO beam control system (Section 2.4).

Section 2.4 discusses various applications and their experimental results. Some of these results have been published in a peer reviewed paper. A copy of the paper is joined as Annex A.

This report also discusses the results of an experimental study of the effects of atmospheric turbulences on the filamentation process (Section 3).

Section 4 discusses the possibility of using the closed-loop correction of the laser beam by the AO system in view of compensating for the effects of atmospheric turbulences.

2   THE ADAPTIVE OPTICS BEAM CONTROL SYSTEM

The formation of filaments suitable for atmospheric studies at long distance remains an issue; a system to adequately control the onset of filaments at atmospheric-scale distances has to be designed.

The laser pulse intensity at which air ionization, and thus filamentation, could start to occur is in the order of 10^{12} W/cm^2 [12]. The distance at which this intensity will be reached by a laser pulse can be controlled in various ways: initial laser beam diameter, beam shape, beam divergence, pulse duration and pulse chirp. Chirped pulses can be obtained by use of either two gratings setups or spatial light modulators [20].

Rodriguez *et al.* [21] reported the observation of filamentation processes at vertical heights as large as 2 km with proper use of a telescope to vary the beam divergence and of different values of negative pulse chirps. The chirp was being varied by moving one of the compressor's gratings with respect to the other in a 2 gratings setup. Jin *et al.* [22] reported controlling precisely the filamentation onset between 7 and 20 meters by varying the beam divergence and/or the initial laser intensity. The variation of the beam divergence was operated by properly controlling the actuation of a deformable mirror.

Liu et al. [23] proposed a method to properly control the filaments at long distances that combines beam expansion and geometrical focusing. The device consisted of a 5 cm diameter convex mirror, whose focal length is −50 cm, and a focusing lens with focal length of 100 cm (diameter of 8 cm). The focusing lens was installed on a motorized stage, allowing a variable effective focal length. The purpose of the device is to generate energetic filaments at a far distance. Distances up to 100 meters were achieved by this method. In order to counter the unwanted effects of multi filamentation competition for the energy in the reservoir, the pulses's perturbations, which caused an early collapse of the filaments, were stretched by increasing the beam diameter with the convex mirror. This process delays the onset of filaments by reducing the self-focusing effects of hot spots in the initial spatial intensity distribution. The position and focal length of the converging lens is adjusted so that the geometrical focus is much shorter than the non linear focus. This means that all the energy contained inside the reservoir is merged around the geometrical focusing area where a sudden generation of strong constructively interfering filaments occurs. However, as the focusing distance increases, the validity of the approximation is not accurate anymore. In fact, because of the limited lens aperture, the difference between the self focal and geometrical distances becomes larger for longer focal distances and leads to multi-filament competition. In an attempt to increase the filamentation onset distance, a new telescope that could further increase the beam diameter was designed.

In a similar approach they called the double-lens setup, Eisenmann *et al.* [24] report results wherein filamentation was made to start at controlled distances between 16 meters and 330 meters. In this experiment, the presence or absence of filaments was

characterized from ablation on solid PVC material (damage threshold $\approx$ 1.2 x 10^{13} W/cm^2).

The research reported here extends the works by Liu *et al.* [19] by pairing a variable focal length telescopic beam expander with an AO system for compensating against wavefront aberrations. The AO system is comprised of a wavefront sensor (WFS) and a deformable mirror (DM). In what follows, the beam expander and then the AO system are first presented. Then, experimental results obtained with them are discussed.

2.1   The focusing beam expander

Figure 1 presents the optical configuration used for the preliminary tests with the AO system. The focusing beam expander of variable focal length consists of a convergent off-axis parabolic mirror (PM) with a metallic coating and a divergent dielectric spherical mirror (CM), mounted on a translation stage, coated for high reflectivity at 800 nm. The former has a diameter of 15 cm, a focal length of 150 cm and its radius of curvature is placed 23 cm away from the mirror's axis. Depending on CM's focal length, the focusing beam expander, with collimated input and output, can either have a magnification of 4X when f_{CM} = -35 cm, or 3X, when it is -50 cm. Unless specified otherwise, CM has focal length f_{CM} = -50 cm and the beam expander is a 3X.
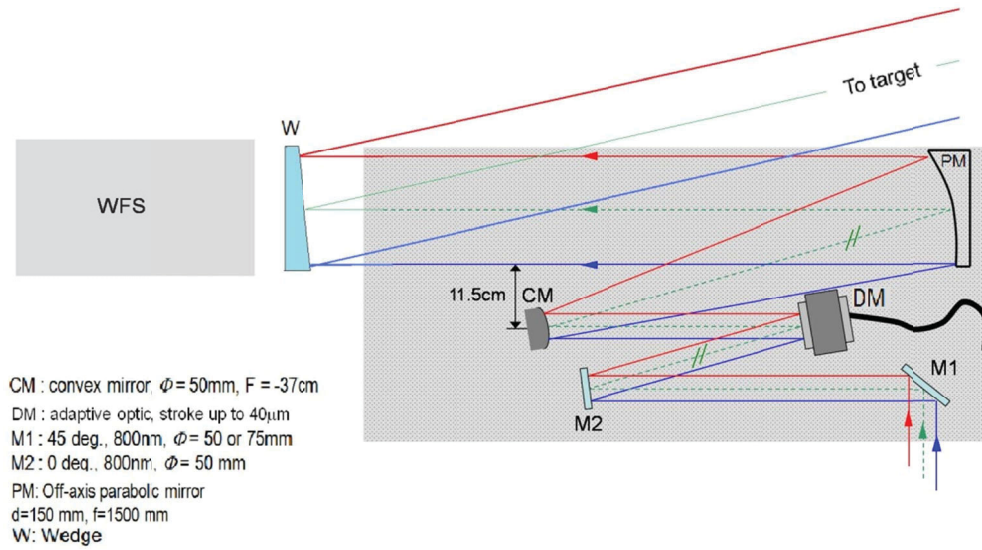
Figure 1: Schematics of the focusing beam expander with AO System

The focal length of the telescope can be modified with a displacement of CM with respect to PM. The deformable mirror (DM) is placed immediately before the focusing beam expander and moves along with CM on the translation stage. The system is configured so that when the focal length of the focusing beam expander is modified, the pointing of the laser beam is maintained constant. This can be realized by keeping the segments M2-DM

12

and CM-PM parallel during the displacement of the translation stage. Therefore, the movement of the stage is collinear with the beam output while the segment DM-CM is at 15 degrees with respect to this axis.

2.2　The AO system

As stated earlier, the AO system is comprised of a wavefront sensor (WFS) and a deformable mirror (DM). Both are operated in a closed loop mode wherein the output from the WFS is used as the error signal to be corrected by proper actuation of the DM.

2.2.1　The Wavefront sensor (WFS)

The entrance aperture of the wavefront sensor (WFS) is positioned behind a 10 cm diameter dielectric wedge (W, fig.1), whose reflecting surface is coated for high reflectivity at 800 nm at normal incidence. The pulses' energy transmitted through the other interface is imaged on the WFS detector's surface. Since the wedge is the last optical component before the target, the system's total aberrations can be measured.

The wavefront sensing device used in these preliminary tests is of type Shack-Hartmann. It consists of an array of lenslets (LA) of the same focal length (size of array: 40 x 40, $d_{lenslet} = 250$ µm, $f_{lenslet} = 14$ mm). Each is focused onto a CMOS detector. The local tilt of the wavefront across each lens can then be calculated from the position of the focal spot on the sensor. Any phase aberration can be approximated to a set of discrete tilts. Figure 2 presents the typical response of a Shack-Hartmann detector. By sampling an array of lenslets, all of these tilts can be measured and thereafter used to reconstruct the wavefront. The local phase shifts are calculated with respect to the Shack-Hartmann's response of a collimated beam without aberration, measured previously and saved in the software's memory.
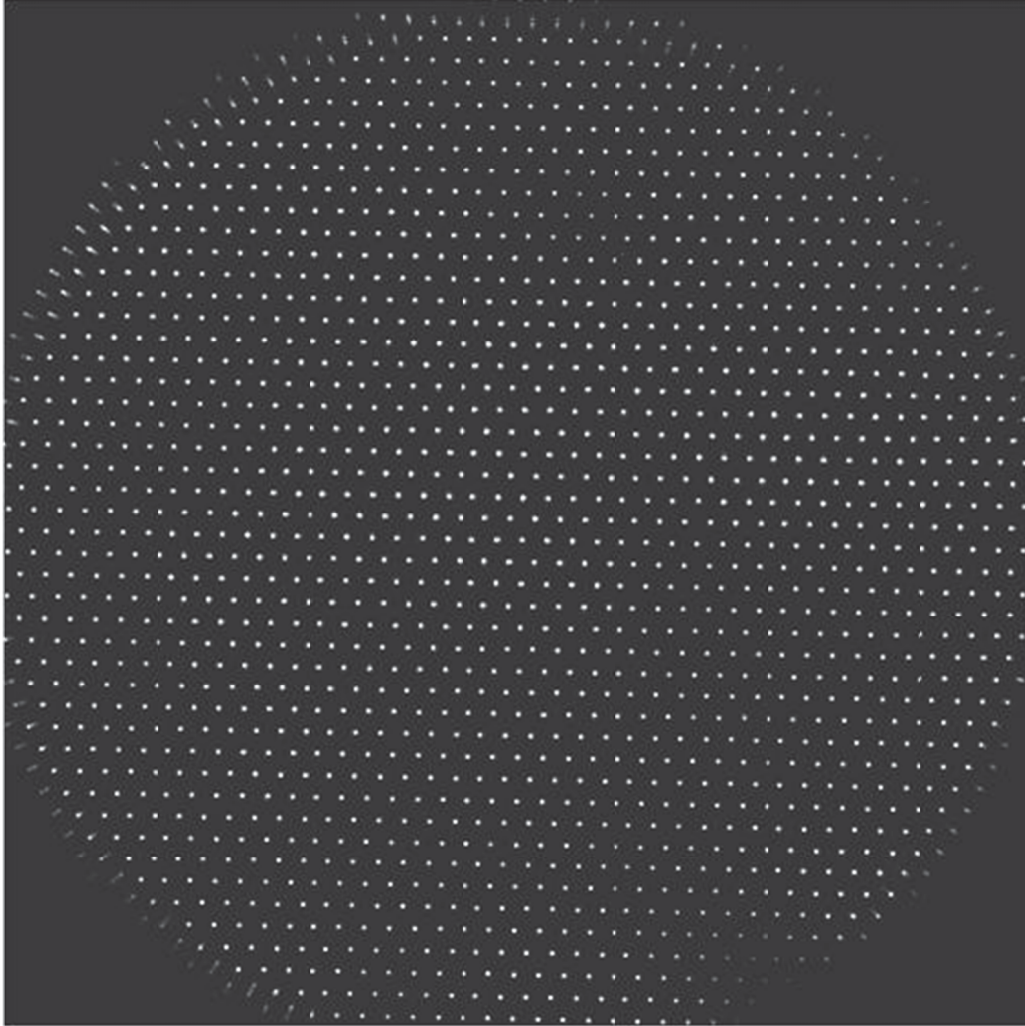
Figure 2: Typical Shack-Hartmann pattern

Figure 3 presents the various components of the WFS tested. Because of the limited size of the Shack-Hartmann detector (LA and CMOS), the input beam is downsized with a telescope consisting in a combination of 2 lenses, L1 of diameter 90 mm and focal 630 mm, and L2 of diameter 25 mm and focal 40 mm. Two dielectric flat mirrors, M1 and M2, coated for high reflectivity at 800 nm, are used to superimpose the input beam and the WFS axis. The Shack-Hartmann detector and L2 are mounted on a translation stage which moves along this axis. The movement of this translation stage, when properly aligned, should only modify the amount of defocus measured by the WFS.
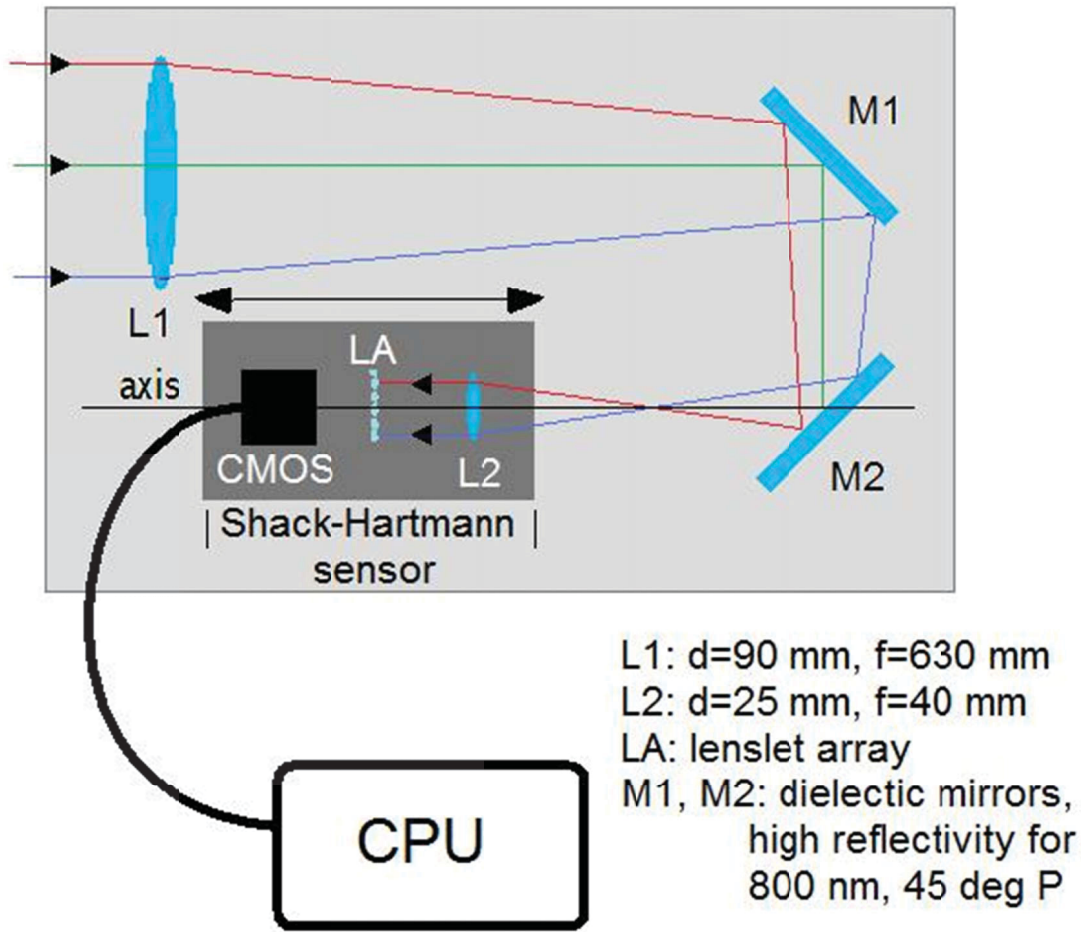
Figure 3: Schematics of the wavefront sensor

The output of the CMOS camera is delivered to a computer where its signal will be analyzed for wavefront correction.

IMPORTANT: The camera has to be protected at all times by its protective cap or by sufficiently dense ND filters.

2.2.2   The Deformable Mirror (DM)

The structure of the bimorph deformable mirror ordered from Night N (opt) Ltd is presented in figure 4a. It is a flat mirror of diameter 55 mm. Two superposed piezoceramic crystals, who share common ground at the interface, are fixed under a glass substrate whose other surface is coated for high reflectivity of 800 nm at normal incidence. The DM's maximal deformation is characterized by a stroke of 40 μm. The top piezo-disc, which is activated by a circular electrode sandwiched between the substrate and the disc, serves for curvature deformation of the mirror. If the beam is properly

centered on its surface, it will only affect the general defocus of the beam. The lower layer is subdivided into 31 segments disposed as in figure 4b, where each sector represents the shape of the activation electrode. Each of these actuators is excited individually with voltages ranging from -300 V to 300 V, applied by a control unit connected via USB to the computer. The voltages can be applied manually or automatically via the closed loop software designed by Night N (opt) Ltd.
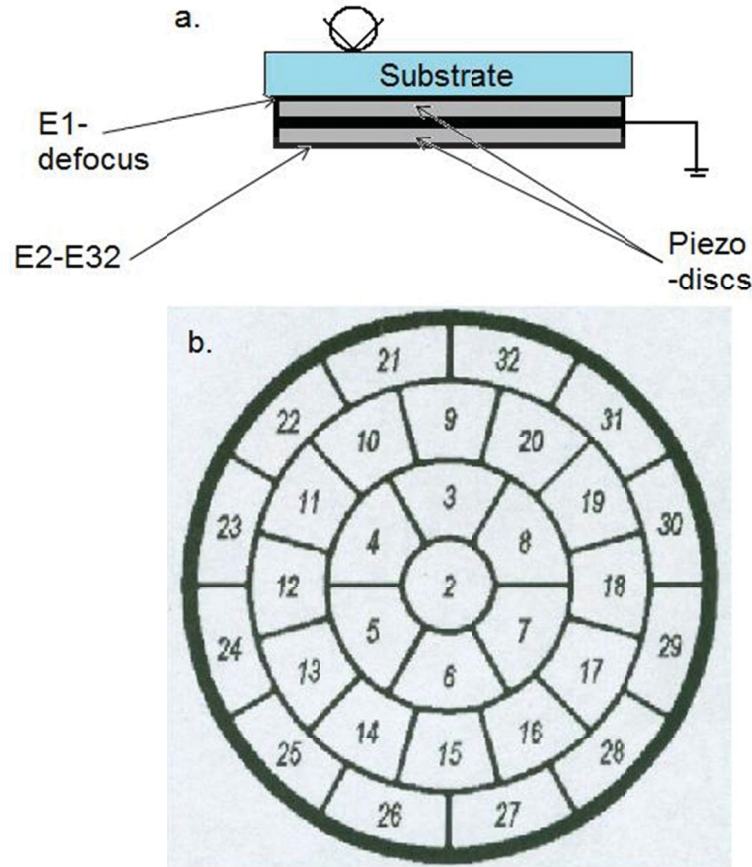
Figure 4: Deformable Mirror

4a) Deformable mirror's structure

4b) Electrode pattern of the piezo-disc E2-E32

2.2.3   Closed-loop wavefront correction

The Shack-Hartmann's camera output and the AO control unit are connected to the computer via firewire and USB, respectively. The software works in a closed-loop configuration with both components, correcting errors until the Shack-Hartmann's CMOS camera observes an array of spots corresponding to a reference saved in the computer. This reference is usually measured from a calibrated, collimated source of the same wavelength as the beam to be corrected. However, it is possible to measure and store multiple reference files that can be used for different focusing distances or generate

specific aberrations. All the aberrations shown by the software (defocus, astigmatism, coma, etc) are calculated with respect to the loaded reference.

Once the reference is selected, the response of the deformable mirror's actuators has to be characterized. For this procedure, each actuator is excited, and the wavefront's deformation is stored in the software's memory. These so-called response functions are used later on as basic responses for the wavefront correction.

This calibration procedure has been applied by the technical personnel of the vendor company Night N. Hereafter, the procedure is described.

2.2.4 The AO system installation by Night N's scientists

2.2.4.1   Procedure for the WFS calibration

The WFS is calibrated with the collimated light source as presented in figure 5. A laser diode is tightly focused through a pinhole (d = 50 μm or d = 15 μm) with a microscope objective of 10X magnification. Two metallic flat mirrors, M1 and M2, guide the divergent beam to an off-axis parabolic mirror of focal length 1 m. A Murty shear plate interferometer is used to verify the output beam's divergence which is adjusted by moving the parabolic mirror along the beam axis.
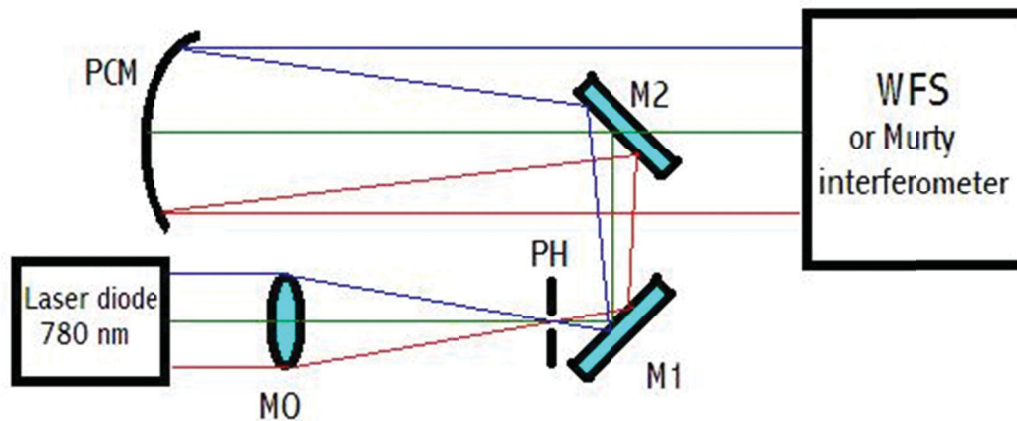
MO: Microscope objective, 10x
M1, M2: Flat metallic mirrors
PCM: Off-axis parabolic mirror f =1 m
PH= Pinhole, d=50 um or 15 um
WFS: Wavefront sensor

Figure 5: Collimation of laser source for WFS calibration

Once the source is collimated, the output is aligned through the WFS. In order to facilitate the task, a circular aperture, centered on the beam, is inserted before the WFS to reduce the source's diameter. Using an IR viewer and a specially designed target fitting L1's surface (fig.3), the WFS is placed so that the reduced beam is superimposed on L1's axis. Another specially designed target, centered on L2, is placed on the Shack-Hartmann's protective cover. M1 and M2 (fig.3) are then used to align the imaged beam along the movement of the translation stage, centered on the target. This procedure can be facilitated by superposing a He-Ne laser at 632 nm to the infrared light for a preliminary alignment with visible light.

The Shack-Hartmann's pattern can be viewed using the closed-loop software. The reduced beam's image is then centered on the CMOS camera using the tilting screws located on the detector's side (fig.3). Before going any further, move the translation stage to verify that the beam is aligned along its axis: if it is so, the beam should not be displaced sidewise.

While performing a phase measurement with the software, the defocus is eliminated by adjusting the distance between L1 and L2. In this case, if the source is really collimated and all the previous steps have been respected, it will indicate that the WFS is correctly aligned. Then, the reference can be measured and stored for the correction of collimated beams (See owner's manual). It is of crucial importance that the calibrated source's diameter be similar to that of the beam to be corrected.

IMPORTANT: The camera has to be protected at all times by its protective cap or by sufficiently dense ND filters.

2.2.4.2   Procedure for the WFS installation

During the installation of the WFS in the focusing beam expander, the calibrated WFS's alignment must not be modified. The WFS is positioned behind the wedge (W, fig.1) and, once again, the specially designed targets used previously and the IR viewer are used. It is also strongly recommended to reduce the beam size with a centered circular aperture placed just before the WFS.

Once the beam is correctly aligned in the focusing beam expander, the reduced beam is centered on L1 using the concentric target. Afterwards, the front part of the WFS has to be fixed on the optical table. Then, the imaged point is centered on L2's target by moving the rear of the WFS and the back part is fixed on the table. Unfix the front end of the WFS and iterate these adjustments until it is perfectly aligned.

The Shack-Hartmann's CMOS camera is connected to the laptop via USB to allow wavefront analysis using the software. The alignment on the CMOS camera is facilitated using the reduced beam. If it is not centered horizontally on the screen, the rear end of the WFS can be moved gently. If it is not centered vertically, the alignment of the focusing beam expander has to be modified. Once the Shack-Hartmann is aligned along the beam axis, the central spot position will no longer change when the translation stage moves

longitudinally. The aperture can now be opened to verify that the whole beam fits the CMOS sensor correctly.

IMPORTANT: The camera has to be protected at all times by its protective cap or by sufficiently dense ND filters.

2.2.4.3   Procedure for the DM installation

The deformable mirror is positioned at DM (fig.1). The top of the mirror is indicated by a metallic pin in the connector's socket. Once the mirror is properly installed in the mount, it can be connected to the control unit's cable.

During the alignment, the beam should be centered on the mirror's surface. For a normal incidence scenario, a hole is punched in the center of the mirror's protective cap as a reference. However, the mirror is positioned at a slight angle which makes this reference useless for the horizontal axis (the vertical reference can be trusted).

IMPORTANT: To install the cable on the mirror, push it gently a few millimeters into the socket and then turn the fixing knob until it is blocked. Repeat these two operations until the cable is in place. Do not use excessive strength during the cable installation.

2.3   Experiments for characterizing the AO system

Two series of experiments have been performed: the first series would only monitor the shape of the wavefront with and without the AO system being engaged; the second would monitor the quality of the filamentation process with and without the AO system being engaged. The quality of the filamentation process is assessed, in the second series of experiments (section 2.4), by measuring the fluorescence from the N_2 species. In this section, we cover the experiments performed to characterize the AO system *per se*.

2.3.1   Controlling the beam pattern

The laser pulses (15 mJ, 5 ps (-) chirp) are launched into a 30 m long corridor, with reflectors (3 dielectric mirrors coated for high reflectivity at 800 nm at normal incidence) at both ends, which provide ~120 m long propagation. The focusing beam expander's translation stage is positioned 216.4 mm from its home so that the focal spot's size is minimized at the end of the propagation distance. Figure 6a and 6b present typical uncorrected and corrected laser shots, respectively, measured 120 m after the telescope. The RMS aberrations measured by the WFS in both cases are, 4 μm (a) and 0.2 μm (b). Obviously the AO system seems to be correcting something, but it is not the focal spot!
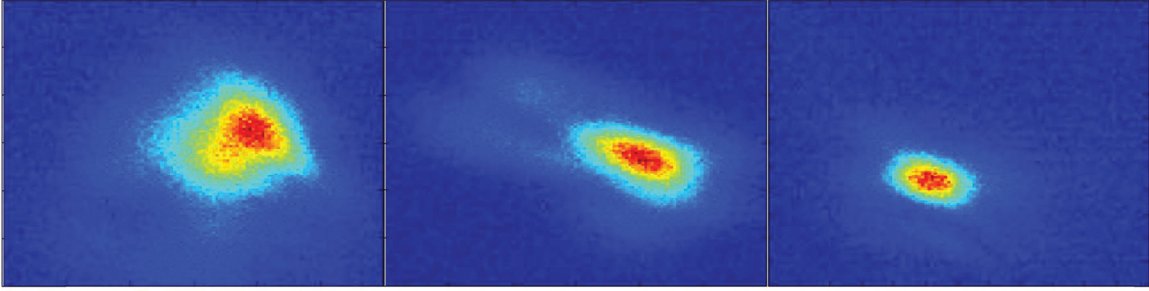
Figure 6: beam patterns measured at 120 m

of wavefronts a) uncorrected, b) corrected by software and c) manually corrected

Figure 6c presents a beam pattern manually optimized. This tedious procedure consists in iteratively applying voltages on the actuators in order to find the best beam pattern. This task has been accomplished by a scientist from Night N and took him approximately 1 hour to do. However, this result shows that the DM can partially correct the wavefront, but the closed-loop system does not provide the best expected results. *Why is it so?* In what follows, various possible explanations are discussed.

2.3.1.1   Possible ameliorations to the AO system

AO system corrects to a flat wavefront

As specified earlier, the software is designed to correct the wavefront in order to reproduce a loaded Shack-Hartmann reference. The loaded reference in this case corresponds to a flat wavefront measured from a collimator (fig. 5) which causes some problems since the desired wavefront has to be spherical and convergent instead.

Moreover, because the wavefront sent to the WFS is convergent and the reference is flat, mainly defocus is measured and since all the actuators work hard to compensate it, the other aberrations may not be corrected efficiently.

This problem could be corrected by two different methods:

-*Multiple references could be loaded depending on the desired focal distance*
   In this scenario, a measured reference (or virtually generated) could be loaded in the software depending on the desired focal distance. Therefore, the AO system would correct to a wavefront with the proper curvature.

-*The Shack-Hartmann's translation stage can be moved to eliminate the defocus*
   This design could be applied in the case of a perfect alignment of the translation stage with respect to the axis shown in fig. 3. A displacement of the translation stage will change the distance between L1 and L2 which will in turn modify the curvature of the

wavefront incident on LA (fig. 3). It is possible, for any focusing distance, to position the translation stage so that the measured defocus is zero. This phenomenon is explained in figure 7. In a), the lenses are separated by the appropriate imaging distance and the curvature of the input and output wavefronts are the same. In b), the Shack-Hartmann sensor's stage is moved to eliminate the defocus, bringing the small lens closer to the large lens. In this case, only the remaining aberrations can be measured and corrected by the AO system.
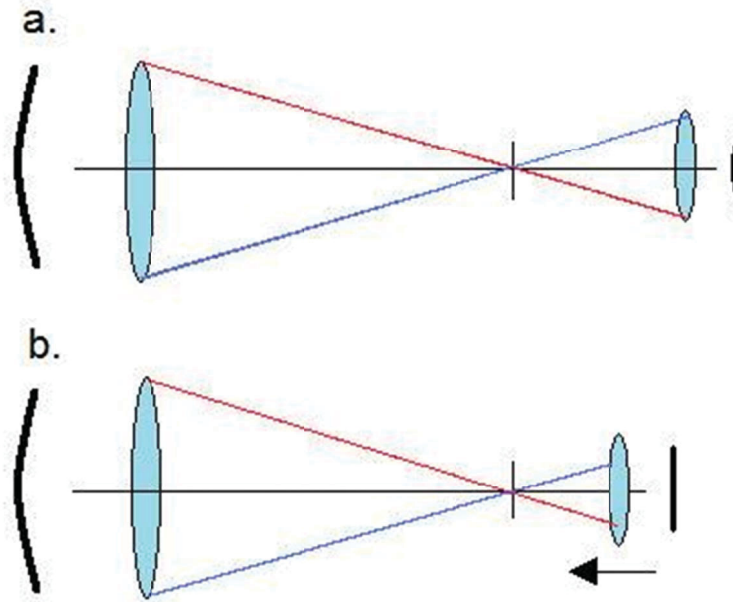
Figure 7: Method to eliminate the defocus measured by the Shack-Hartmann sensor

a) *The distance between the lenses is the imaging distance: the curvature of both wavefronts is the same*

b) *The distance between the lenses is smaller than the imaging distance: a plane wavefront is obtained*

Even though we believe these techniques could be applied, when they were put to the test, no good results were observed.

The beam size incident on DM is too small

The beam used in these experiments is approximately 20 mm at e^{-1} and the active surface of DM is 55 mm in diameter. Therefore, when the beam is centered on the mirror's surface, the outer actuators are excited by high voltages since they do not influence the wavefront significantly. Better correction could be achieved if the incident beam fits most

of the DM surface. Therefore, for the experiments at Laval University, a two-lens telescope has to be designed to enlarge the beam by a factor of 1.5.

The WFS's input aperture is too small

Because the beam's diameter after the telescope is approximately 70 mm at e^{-1}, the 90 mm diameter lens L1 (fig.3) does not collect the entire incoming wavefront. Therefore, some points of the outer Shack-Hartmann's pattern are missing and lead to an error in the correction. This will result in residual aberration, especially in the wavefront's outer part.

The reflection from the wedge's surface is not corrected

The reflection on the wedge's surface (W fig.1) cannot be corrected by the DM since it is not observed by the WFS. Moreover, if the reflective surface caused any wavefront's distortions, the WFS would see an opposite aberration in the transmission. This phenomenon is illustrated (as example) in figure 8 for defocus. If the wedge's surface is slightly concave, an incident collimated beam will be convergent after the reflection, but divergent on the transmission.
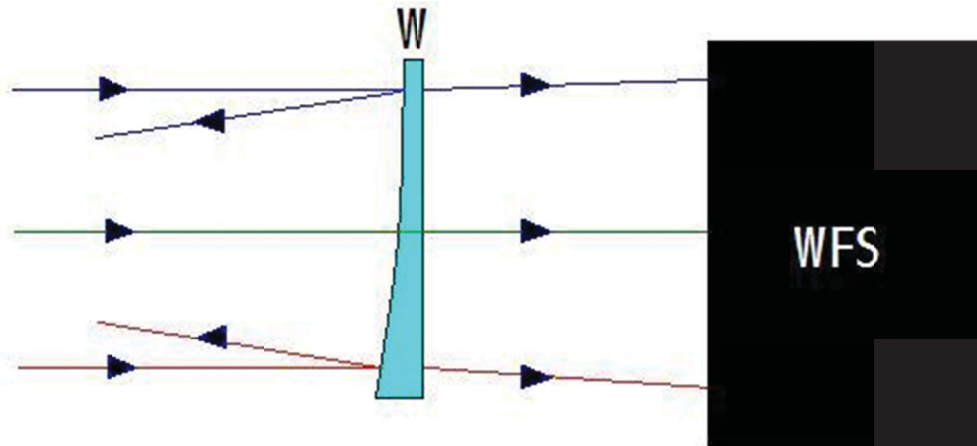
Figure 8: Example of distorsions induced by a wedge whose reflective surface is not flat, on the reflected and transmitted beams

Since large optics with good surface quality are rather expensive and/or difficult to make, we decided to test the quality of our wedge with a Zygo interferometer ($\lambda = 632$ nm). The print screen of the report analysis is shown in figure 9. These results show that the surface has a strong defocus (4th Zern) and significant amount of astigmatism that cannot be corrected by the AO system (5th and 6th Zern). The accumulated uncorrected aberrations from the wedge and the reflecting mirrors at the corridor's ends, certainly enhance the wavefront's distortions in the focal region.

22
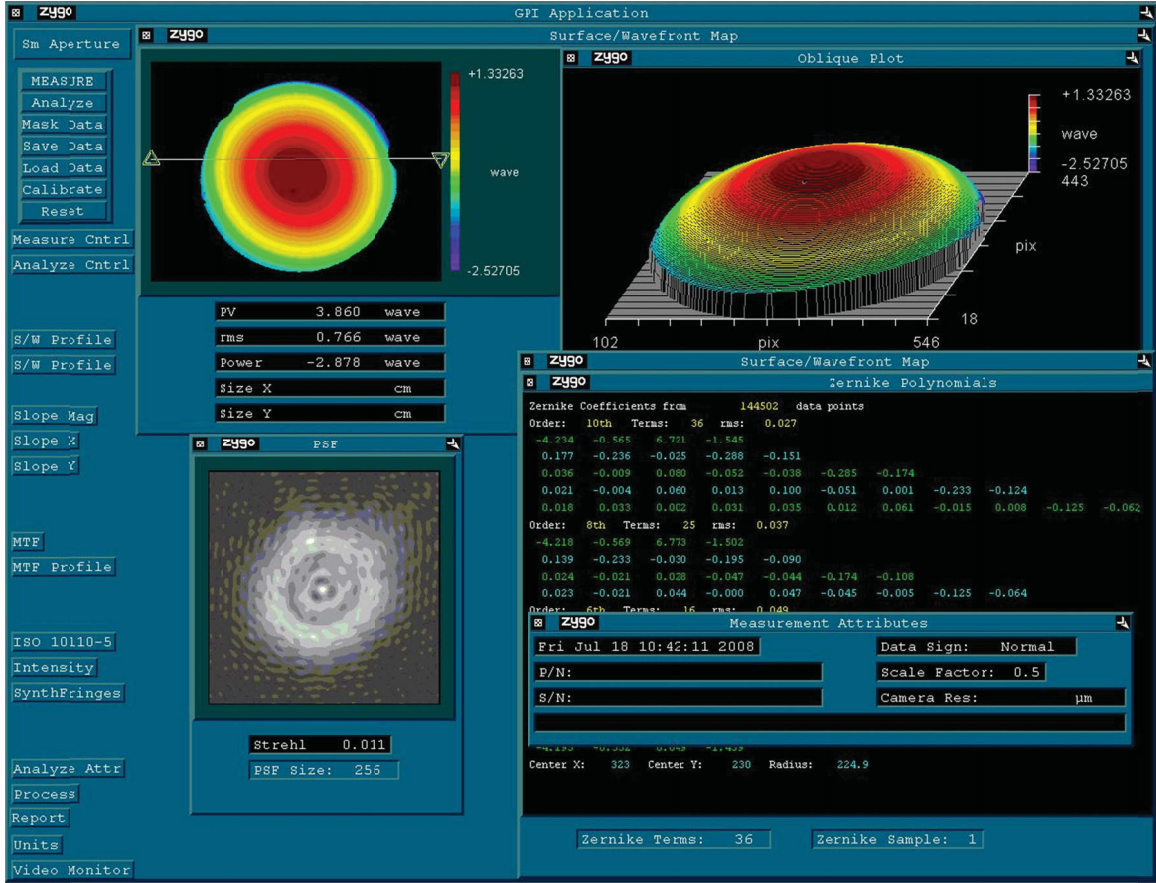
Figure 9: Analysis of the wedge's coated surface by a Zygo interferometer

A method to avoid some of the problems encountered

For these preliminary experiments, it was found that by placing the wavefront sensor behind the dielectric reflector positioned 60 m after the focusing beam expander's output, some of the problems previously met could be avoided. In fact, at this position, all the system's aberrations, including the wedge and the 30 m mirror's reflections are corrected. The only uncompensated effects are the reflections on the mirrors located at 60 and 90 m and the turbulence encountered while propagating from 60 to 120 m. Moreover, because of external focusing, the beam size is smaller than L1 (fig.3) and is entirely collected by the Shack-Hartmann sensor. This ensures that the total wavefront can be corrected.

For this test, the focusing beam expander's translation stage (fig.1) is positioned 216.4 mm from home to optimize the uncorrected focal spot at 120 m. Then, the WFS's Shack-Hartmann sensor (fig. 3) is moved along its axis in order to eliminate the defocus (fig. 7) calculated by the software. Figure 10 presents the beam patterns measured for uncorrected (a.) and corrected (b.) pulses. Even though the position of the focusing beam expander's translation stage is the same for figures 6a and 10a, the beam patterns are totally different. This is most probably due to a better alignment of the system for the latter.
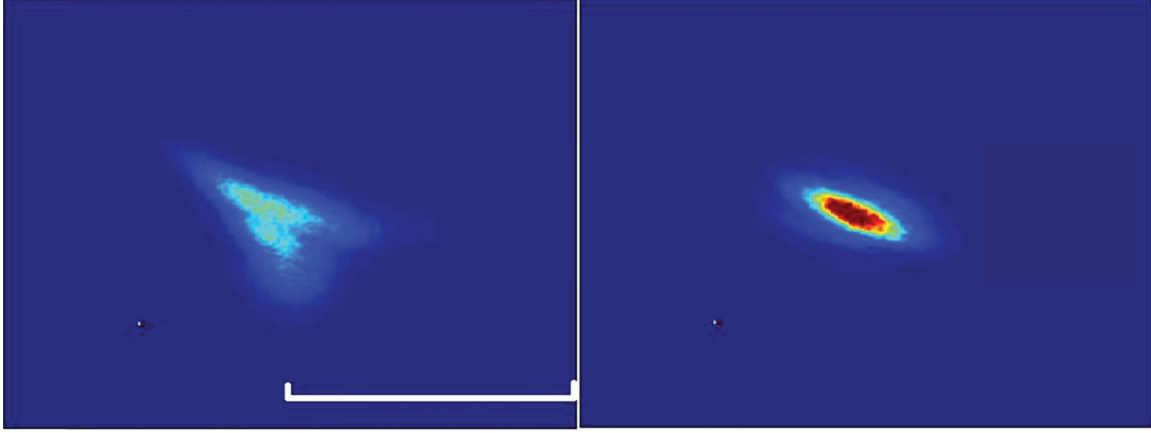
Figure 10: a) uncorrected and b) corrected beam patterns with WFS located behind the mirror at 60 m

This time, a clear amelioration of both the pattern and intensity of the focal spot is observed when the correction is applied. It is important to note that for figure 10b, the focal spot size has been reduced by a fine tuning of the Shack-Hartmann sensor's position (figs. 3-7). Indeed, since the software always corrects to observe a plane wavefront in front of the lenslet array, a change in the distance between L1 and L2 during correction, induces a modification of the focal length. In theory, if the stroke of the DM is sufficient, no movement of the translation stage of the focusing beam expander is necessary to modify the system's focal length. This could be replaced by a simple movement of the Shack-Hartmann along its axis. The advantage of this technique consists in minimizing the alignment of the focusing device.

2.4   Experiments with the AO system for remote sensing applications

This AO system (AOS) configuration was then put to a test to verify whether it could enhance the results obtained for specific applications of filamentation. These tests were performed in Professor See Leang Chin's Laboratory in Laval University, who is a specialist in remote sensing with laser filaments. The AO system was put to the test and its incidence on the returned signals was checked for various targets.

2.4.1 Detection of atmospheric N_2

The AOS was first tested to measure N_2 fluorescence signals from ambient air in the laboratory. A PMT based LIDAR configuration has been used to characterize the plasma distribution of the formed filaments for the case of uncorrected and corrected wavefronts. The pulse energy was 70 mJ and the pulse duration was set to 3 ps, negatively chirped. Fig. 11 presents, for (a) uncorrected and (b) corrected wavefronts, 500 backscattered traces from individual laser shots. Each plot has for horizontal scale the distance from the focusing beam expander. The vertical scale corresponds to the number of the trace recorded and the color scale is the N_2 signal intensity. This plot shows that both the amount of fluorescence produced by the filaments and the shot-to-shot stability were

improved when the wavefront correction was applied. Moreover, the location of the filament (by looking at the highest signal intensity) was also stabilized.
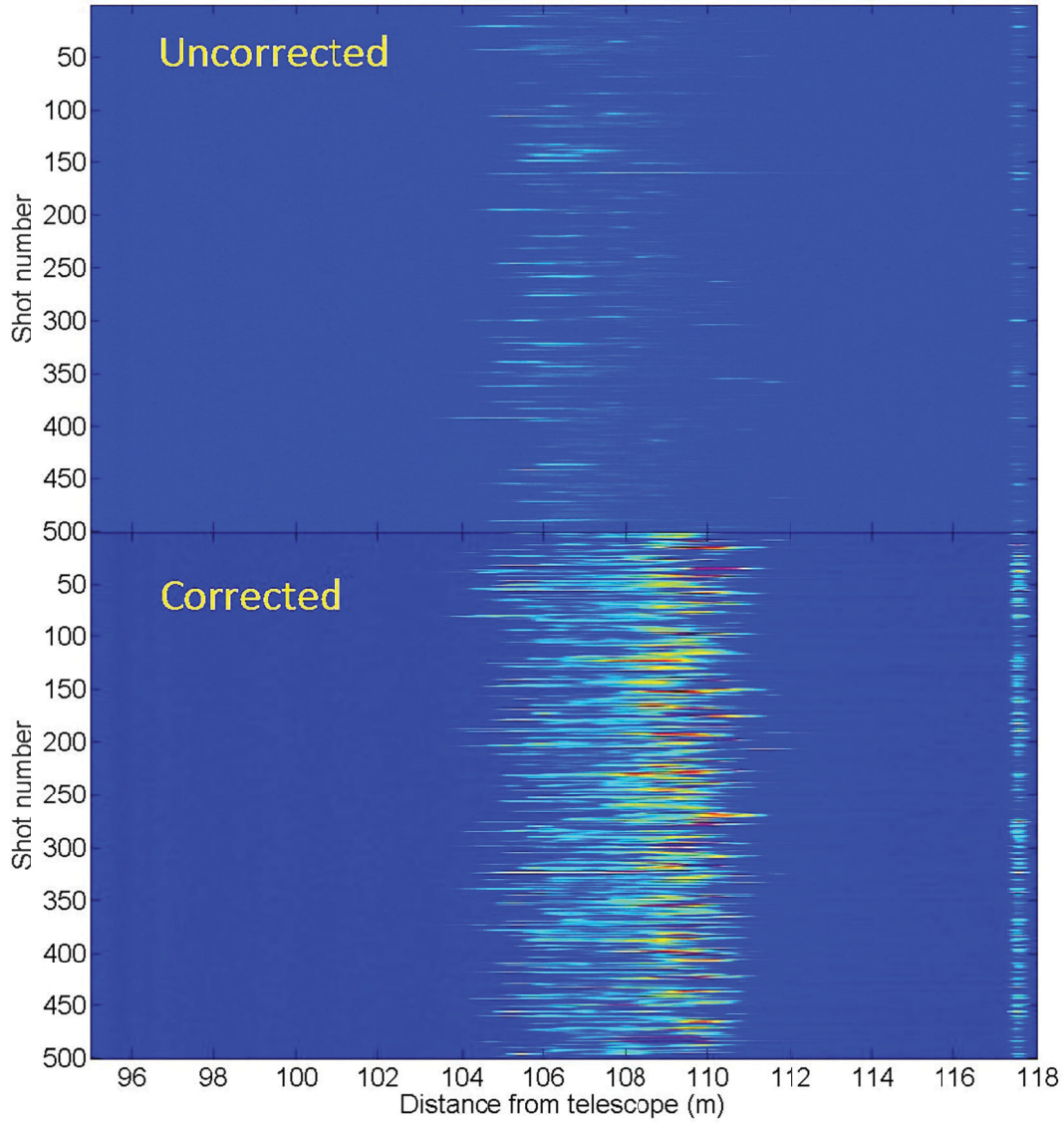
Figure 11: 500 consecutive LIDAR traces in the case of a) uncorrected and b) corrected laser pulses

The standard deviation for the location of the peak intensity of the 500 corrected traces was reduced by 23% with respect to the uncorrected ones. The two curves presented in Fig. 12 correspond to the sum of the 500 traces shown in the previous Figure for the uncorrected and corrected wavefronts. The AO system improved the overall integrated signal by a factor of 7.
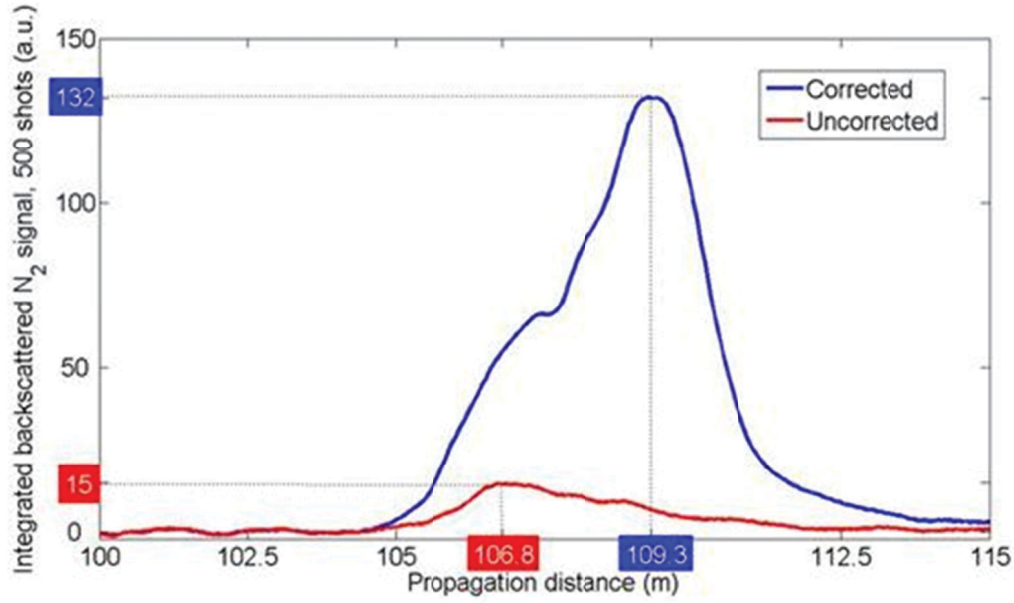
Figure 12: Accumulated LIDAR traces from figure 11 for uncorrected (red) and corrected (blue) wavefronts

The PMT setup was replaced with the spectrometer/ICCD assembly. In order to get enough signals for the ICCD, the pulse energy was increased to 85 mJ and its duration shortened to 2 ps, negatively chirped. The gated detector was triggered slightly before the formation of the filaments and the gate window was opened for 30 ns. The spectra in Fig. 13 are the results of 100 accumulated laser shots for the case of (a) uncorrected and (b) corrected wavefronts. When the AOS was turned off, (Fig. 13a) only the 800 nm scattering could be measured. This indicates that the signal observed with the PMT in Fig. 13a is very weak N_2 signal. When the AOS was used, strong N_2 bands were observed (Fig. 13b). The previous results indicate that the wavefront correction has a strong enhancing effect for remote sensing of atmospheric gas samples.
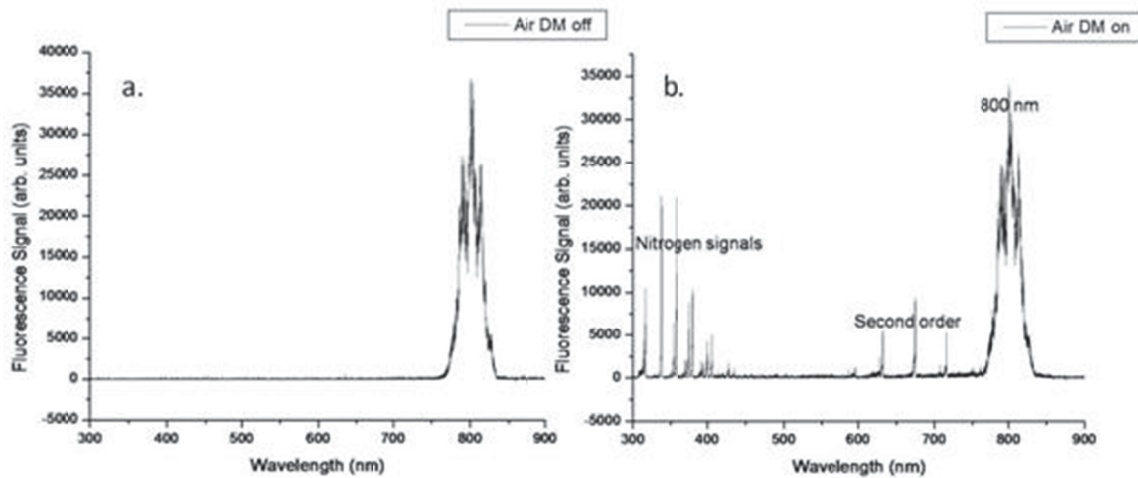
Figure 13: Backscattered spectra measured with the spctrometer/ICCD assembly, for a) uncorrected and b) corrected wavefronts.

26

2.4.2 Remote sensing of hydrocarbons in air

Three hydrocarbon gases, namely methane (CH_4), acetylene (C_2H_2) and ethylene (C_2H_4), were tested. Each sample consisted of a mixture of 2% of hydrocarbon gas balanced to atmospheric pressure with air. The mixture was then injected into a 2 m long metallic tube with opened ends which was placed at the filaments' zone (110 m after the focusing telescope). The middle part of the pipe had an exit which was connected to the ventilation to ensure a continuous renewal of the gas mixture. The energy of the laser was 85 mJ with a pulse width of 2 ps negatively chirped. One after the other, the gases mixtures were injected in the tube and the CH emissions, resulting from the interaction with the filaments, were recorded. The spectra of pure air (red) and contaminated air (black) are presented in Fig. 14 for a) 2% C_2H_2, b) 2% C_2H_4 and c) three different concentrations of CH_4. Because no signal could be obtained without wavefront correction, all the spectra were measured with an active AO system. At 2% concentration, the CH band could be detected and identified for all the tested gas mixtures and the strongest CH signal was obtained for C_2H_2 (Fig. 14a). As shown in Fig. 14c, three different concentrations of methane mixtures were available and tested. Even at the lowest available concentration, 0.5% CH_4 in air, CH emission band could be identified and an extrapolation of the integrated CH signal indicates that, in these experimental conditions, the minimal concentration of methane that could be measured, in this configuration, would be approximately 0.34%.
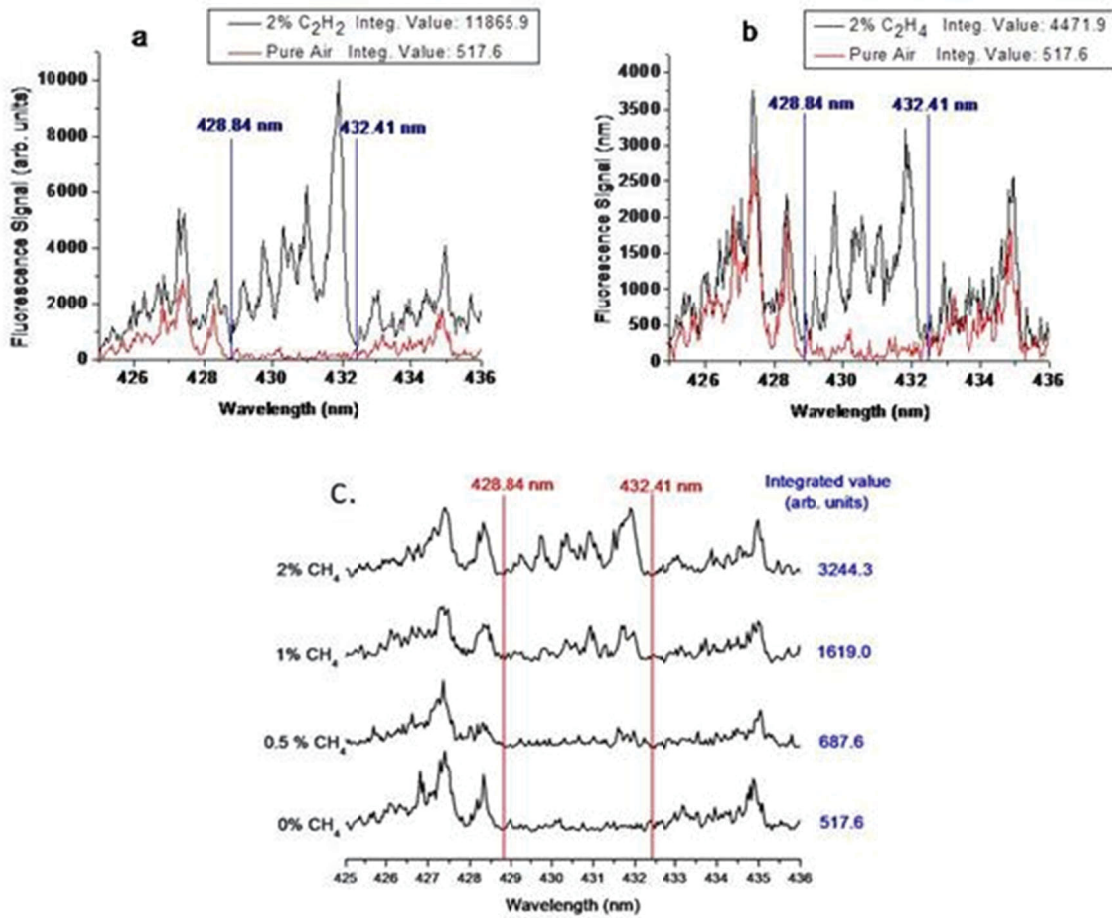
Figure 14: Filament emissions spectra of a) pure air (red) and contaminated with 2% C_2H_2 (black), b) pure air (red) and contaminated with 2% C_2H_4 (black) and c) CH_4 in different concentrations of 0 to 2%. Integrated values of the CH band between 428.84 nm to 432.41 nm are used to characterize the hydrocarbon signal strength.

2.4.3. Probing a solid lead sample

The gas tube was then replaced by a lead target mounted on a rotating motor located 118 m after the focusing telescope. The focal length was adjusted to obtain a strong filament interaction at the target's location. The sample's rotation ensured that each oncoming laser pulse hits on a fresh surface. In order to avoid signal degradation due to surface deterioration, the sample's surface was cleaned with a sharp blade before each spectral measurement.

Filaments, formed from 80 mJ/5 ps negatively chirped laser pulses, interacted with the sample and the recorded spectra are shown in Fig. 15 for uncorrected and corrected wavefronts. The temporal gate was opened for 100 ns, triggered 2 ns after the pulse interaction with the target. These results show that, when the wavefront correction was applied, the integrated (350 nm to 575 nm) backscattered signal increased by a factor 6.8. It demonstrates the efficiency of the AO system to increase the backscattered emissions from metallic targets.
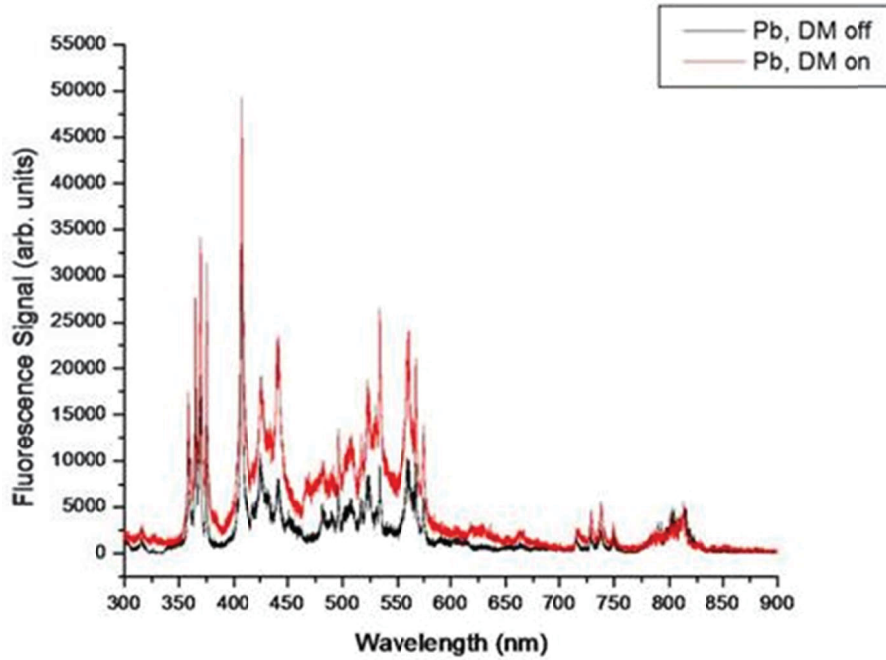
Figure 15: Typical lead spectra measured for uncorrected (black) and corrected (red) laser pulses. The integrated lead signals increases by a factor 6.8 for corrected wavefronts.

2.4.4 Contaminated aqueous aerosols

The last target used in this series of experiments consisted of an aqueous aerosol cloud in which NaCl was dissolved at a concentration of 5 g_{NaCl}/L_{water}. Aerosols were generated by a commercial ultrasonic humidifier, which produced droplets of 10 μm mean diameter, and injected in the same chamber described in reference [25]. The micro droplet density is approximately 300 cm^{-3}.

Filaments formed from the 80 mJ/5ps negatively chirped laser pulses interacted with the target located 110 m away from the focusing telescope. The backscattered sodium emissions, measured with the spectrometer/ICCD assembly, are presented in Fig. 16 for a) uncorrected and b), corrected wavefronts. In both scenarios, the sodium doublets were easily identified. As expected, the integrated (588.0 nm to 591.5 nm) backscattered signal increased when corrected wavefronts generated the filaments. In fact, the intensity at the core of a grown filament in air is sufficiently high to explode the microdroplet and significantly contribute to enhance the emissions [6].
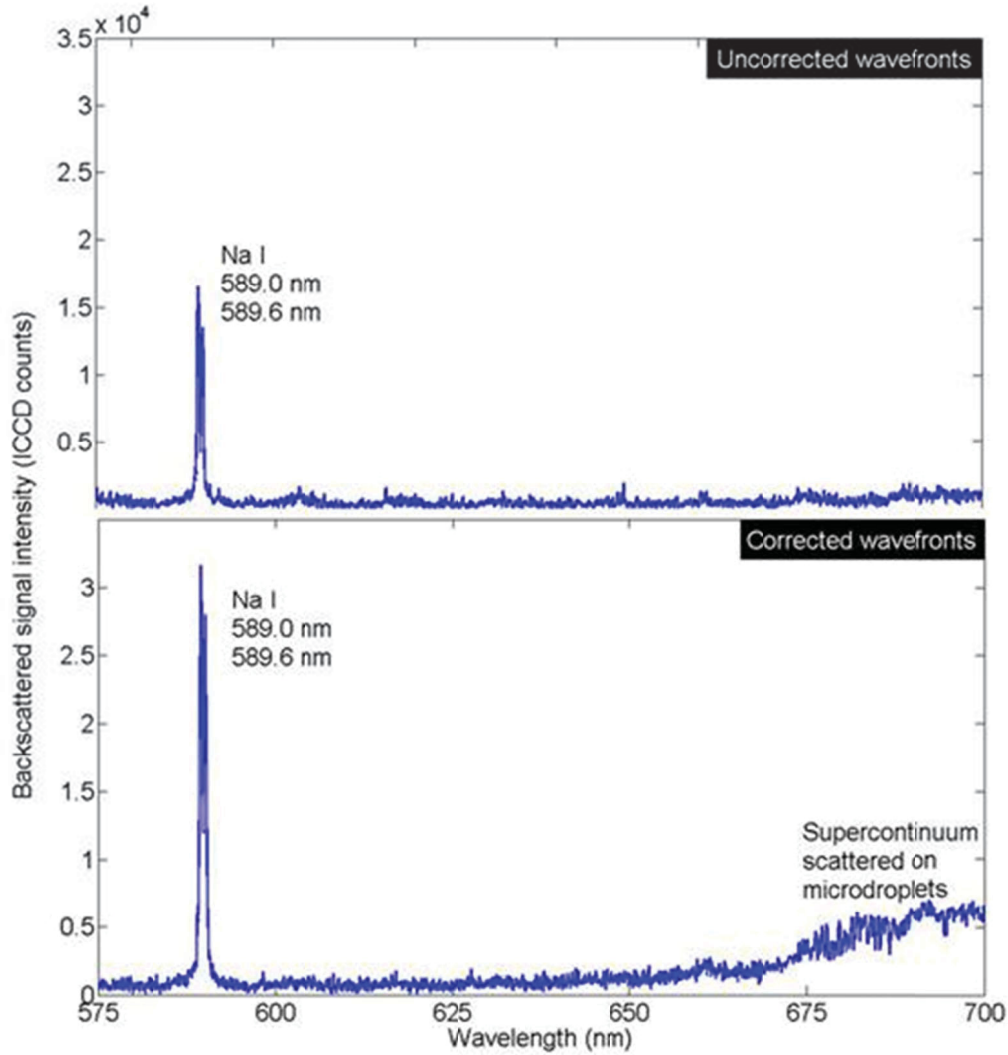
Figure 16: Typical sodium spectra measured from aqueous aerosol clouds with uncorrected and corrected laser pulses. The integrated sodium emission increases by a factor 2.3 for corrected wavefronts.

However, this enhancement factor (2.3) is not as important as for the other targets because the ionization mechanism does not entirely rely on filamentation in air. In fact, the aqueous aerosol cloud can be described as a cloud of micron size and randomly distributed spherical lenses [26]. Each small lens can focus the incident light to nanosized

regions, within the micro droplets, to produce a plasma and fingerprint emissions. Indeed, when an ultrashort laser pulse meets a micro droplet contaminated with NaCl, the light coupling mechanism takes place and Na emissions are produced. As a result, the signal is already strong for uncorrected wavefronts and any enhancement due to filaments formed from the corrected wavefronts becomes limited.

2.4.5 Extrapolation over distance

In the current beam-folding configuration, N_2 fluorescence excited by filaments generated 110 m after the focusing telescope was detected with a LIDAR located 18 m away from the filament zone. Therefore, an extrapolation based on the LIDAR equation [11] has to be performed to verify whether the produced signal is sufficiently intense to be detected at a distance larger than 110 m. Assuming a perfect scenario where only the detection solid angle dependence is influent, the collected signal will decrease as the square of the distance (R) between the LIDAR and the filaments ($1/R^2$). The traces presented in Fig. 12 are used to extrapolate the N_2 fluorescence signal collected at a distance of 18 m for uncorrected and corrected wavefronts. For this calculation, the peak signal intensity is extrapolated, based on the R^{-2} relationship, until it reaches the detection limit which corresponds to the maximum background signal (Fig. 12, 95 m-102 m) plus 3 times the background standard deviation σ.

The results are presented in Table 2.1. This simple calculation demonstrates that the signal produced by the uncorrected wavefronts could be observed at a maximal distance of 32 m whereas the corrected ones could reach 125 m. It corresponds to an increase by a factor 3.9 in probing distance.

	Uncorrected	Corrected
Peak signal (a.u.)	14.6	132.8
Peak signal distance from LIDAR (m)	16.8	19.3
Detection limit, $\text{mean}_{bg} + 3\sigma$ (a.u.)	4.2	3.1
Extrapolation distance (m)	32.1	125.3

Table 2.1: Details of the extrapolation performed for the backscattered traces presented in Fig.12

2.4.6 Perspectives

Even if the previous experiment is not realistic in real field applications, i.e: the WFS cannot be located 60 m away from the laser system, we demonstrated that the AO system can be used to efficiently deliver focused laser pulses at 120 m. The aberrations induced by the wedge's reflection can be solved by replacing this component for one with a better surface quality. However, this component would be hard to produce and very expensive.

Another method consists in using an indirect measurement, other than the wavefront's flatness, to optimize the laser pulses. This indirect signal could be, as an example, the N_2 signal emitted from the filament, remotely collected by a LIDAR. Therefore, instead of optimizing the wavefront, the DM could optimize the fluorescence signal. This technique would avoid any problem caused by surface qualities of the mirrors or the turbulence

present in the propagation path since the AO system would work on the optimization of the filaments' quality.

3   THE EFFECTS OF ATMOSPHERIC TURBULENCES

Several groups investigated the effects of air turbulence on remote filamentation. It is now common knowledge that a strong turbulence source localized prior to filamentation may lead to their destruction [27]. In fact, the *Teramobile* group demonstrated that a turbulence source, characterized with a structure parameter of the refractive index $C_n^2 > 10^{-9}$ m$^{-2/3}$, located 5 m before the filamentation would result in a filamentation shot-to-shot probability lower than 10 %. However, once the filament is formed, the turbulence effect is considerably attenuated. Indeed, they also demonstrated that a turbulence source characterized with a $C_n^2 < 10^{-8}$ m$^{-2/3}$ placed immediately after the collapse point would still allow a 90 % filamentation shot-to-shot probability. In both scenarios, the results are promising since typical atmospheric structure parameters of the refractive index range from $C_n^2 = 10^{-15}$ m$^{-2/3}$ to 10^{-13} m$^{-2/3}$, which is well below the values mentioned above.

In another set of experiments [28], a well calibrated turbulence chamber was used to simulate an extended source of turbulence. They demonstrated that filamentation can be initiated and propagate through strong extended turbulences well above the typical atmospheric values. It was found that a 50% shot-to-shot probability of filament transmission was still obtained for $C_n^2 L < 4.4 \times 10^{-10}$ m$^{1/3}$ where L is the length of the turbulence chamber (1.3 m). Moreover, the transmitted filaments kept their spectral properties including correlations inside the white-light supercontinuum generated through self-phase modulation occurring during filamentation.

More recently, the effects of air turbulence on filamentation were investigated experimentally and numerically for femtosecond pulses with power of a few critical powers for self-focusing [29]. They demonstrated that air turbulence in the path of the beam prior to filamentation induced large beam pointing and formation of instabilities attributed to an increase of the self-focusing distance [23, 30]. In contrast, Kandidov *et al.* [31] found from a numerical simulation that the distance at which the intensity in the non-linear focus reaches the ionization threshold is random for the different laser shots but that, on the average, turbulence should lead to a shorter collapse distance. The principal difference between these two studies is that the latter considered laser pulses of power well beyond the critical power for self-focusing, resulting in multiple filamentation, while the former, with laser pulses slightly above the critical power, observed the collapse of the beam as a whole.

Ma *et al.* [32] investigated numerically the influence of air turbulence on long range filamentation. The results obtained indicated that the diameter of the filaments formed by femtosecond laser pulses propagating freely in the atmosphere, which is normally around 100 microns, could be widened to mm level under air turbulence conditions. This widening effect is caused by phase perturbations of the background energy reservoir which can be accumulated with propagation distance. The 'hot' perturbations induced compete for the energy, which partly breaks the processes of self focusing and energy replenishment from the background reservoir to the filament core. As a result, linear diffraction becomes a significant factor to balance the self focusing nature of the filaments and their intensity is reduced to approximately 10^{12} W/cm^2, which is around the ionization threshold of air. The simulations revealed that the peak electron density produced by the filaments passed from $\sim 10^{15}$ cm^{-3} to ~ 30 cm^{-3} for unperturbed and

turbulent media respectively. This propagation regime is similar to the self-channelling of infrared laser pulses without ionization observed by Méjean *et al.* [33] during an outdoor experiment.

In the present report, the effects of strong and localized air turbulences on filamentation is investigated via the direct observation of the plasma channels left behind the laser pulse. This characterization is performed using a LIDAR system which collects the N_2 fluorescence emitted by the recombination of the ionized molecules. The filamentation instability when the turbulence source is located prior to filamentation is confirmed. However, even though the filaments survive the interaction when the turbulence source is placed in the filament zone, an overall partial extinction of the plasma emissions is observed due to the locally enhanced C_n^2. Moreover, because of the temperature dependent N_2 fluorescence yield, the hot stream of air induces a longitudinal dip located at the position of the 600 °C stream of air.

3.1 Description of the Experimental Setup

In this experiment, the filaments are produced from negatively chirped laser pulses emitted at a 10 Hz repetition rate by a commercial Ti:Sapphire CPA laser system (Spectra-Physics). The collimated pulses propagate through a 5 m distance before hitting an on-axis circular aperture of 4.5 mm diameter. The aperture is inserted in the beam path to stabilize and enhance the plasma emissions [34].

A LIDAR [35] system, looking at the filaments formed in a 20 m long corridor, is used to collect the plasma's fluorescence on the sensitive surface of a photomultiplier tube (PMT, Hamamatsu R7400P). A UG11 filter [36] and a dielectric mirror coated for high reflectivity at 800 nm at perpendicular incidence, are used as a band pass filter for optimal detection of the molecular fluorescence of N_2. Because of the known speed of light, the temporal traces from the oscilloscope can be converted to a spatial scale which allows longitudinal positioning of the produced signal. Considering that the lifetime of the N_2 fluorescence signal is around 1–2 ns [37], the resolution of this detection system, and hence, the longitudinal error in the starting and ending positions of the filament is around 30–60 cm for a single-shot pulse.

Before the aperture, the pulses are characterized with a negatively chirped duration of 100 fs FWHM and energy of 7.2 mJ. The initial beam diameter, measured where the intensity is decreased by a factor e^{-1} with respect to the signal's peak value, is 5.2 mm.

The turbulence source consists in a heat gun (Ungar 1095) providing a continuous stream of air, with an approximate diameter of 2 cm, at a temperature of approximately 600 °C (known from the heat gun's specifications). However, since the hot stream of air was not confined in any sort of enclosure, it increased significantly the surrounding value of the structure parameter around the turbulence source. The structure parameter of the refractive index (C_n^2) was calculated from the data measured with a commercial scintillometer (SLS 20). Based on Clifford's model [38], C_n^2 can be retrieved from the equation:

$$C(\tau) = 4\pi^2 k^2 \int_0^L dz \int_0^\infty dK \, K\varphi \sin^2\left[\frac{K^2(L-z)}{2kL}\right] \qquad (1)$$

where $C(\tau)$ corresponds to the normalized mean autocovariance of the 2 channel scintillometer, k is the wavenumber, L is the propagation distance between the transmitter and receiver (L=28 m) and K is the wavenumber of the turbulent refractive index fluctuations. Based on the Kolmogorov formalism, φ, the refractivity spectrum, can be approximated by the following expression:

$$\varphi = 0.033 C_n^2(z) K^{-11/3} \qquad (2)$$

where $C_n^2(z)$ is the structure parameter of the refractive index. In this experiment, $C_n^2(z)$ takes the form of a rectangular function where the base line corresponds to the C_n^2 calculated when no turbulence source is inserted in the beam path ($C_n^2{}_{NT}$) and the top line is the desired $C_n^2{}_{TS}$ of the turbulence source.

In the situation where no turbulence source is inserted along the beam path, equation (1) becomes:

$$C(\tau) = 4\pi^2 k^2 0.033 C_n^2{}_{NT} \int_0^L dz \int_0^\infty dK \, K^{-8/3} \sin^2\left[\frac{K^2(L-z)}{2kL}\right] \qquad (3)$$

where the integral over z and K ($Integral_{entirePath}$) is evaluated numerically using a standard matlab integration method. Therefore, $C_n^2{}_{NT}$ can be calculated from (3), with the following equation:

$$C_n^2{}_{NT} = \frac{C(\tau)}{4\pi^2 k^2 0.033 Integral_{entirePath}} \qquad (4)$$

We calculated that the structure parameter of the refractive index for the non turbulent medium is $C_n^2{}_{NT} \approx 10^{-17}$ m$^{-2/3}$.

On the other hand, when the turbulence source is inserted in the beam path, equation 1 becomes:

$$C(\tau) = 4\pi^2 k^2 0.033 \left\{ C_n^2{}_{NT} \int_0^L dz \int_0^\infty dK \, K^{-8/3} \sin^2\left[\frac{K^2(L-z)}{2kL}\right] \right.$$
$$\left. + C_n^2{}_{TS} \int_{turbStart}^{turbEnd} dz \int_0^\infty dK \, K^{-8/3} \sin^2\left[\frac{K^2(L-z)}{2kL}\right] \right\} \qquad (5)$$

where the integration limits of the second integral correspond to the starting point of the turbulence zone (*turbStart*) and the ending position (*turbEnd*). Again, both integrals are

evaluated numerically to obtain Integral$_{entirePath}$ and Integral$_{turbZone}$. Therefore, $C_n^2{}_{TS}$ can be evaluated from (5) using the following equation:

$$C_{n\,TS}^2 = \frac{C(\tau)}{4\pi^2 k^2 0.033 Integral_{turbZone}} - C_{n\,NT}^2 \frac{Integral_{entirePath}}{Integral_{turbZone}}$$

(6)

Here again, $C_n^2{}_{TS}$ is considered constant on the whole length of the turbulence source (*turbEnd – turbStart* = 2 cm) and its approximate value is $C_n^2{}_{TS} \approx$ 5 x 10^{-10} m$^{-2/3}$.

However, it was found that the heat gun increased the surrounding value of the structure parameter in an approximate radius of 1 m around the turbulence source. In fact, a temperature increase of 0.2 °C, with respect to the laboratory nominal temperature, could be measured 1 m away from the hot stream of air. Therefore, in order to evaluate the average structure parameter of the refractive index surrounding the heat gun, we considered the situation where $C_n^2{}_{TS}$ is constant over a distance *turbEnd – turbStart* = 2 m and obtained $C_n^2{}_{TS} \approx 10^{-13}$ m$^{-2/3}$. Because of the small dimension of the turbulence source with respect to the scintillometer's laser propagation length, the error on the measurements of $C_n^2{}_{TS}$ is ~50 % and leads to an overestimation of the computed structure parameter. This error, computed form C_n^2 fluctuations for multiple and identical consecutive measurements, seems significant, but compared to the difference of multiple orders of magnitude between $C_n^2{}_{NT}$ and $C_n^2{}_{TS}$, it is rather negligible.

3.2   Results

The heat gun was inserted at different positions along the short pulses propagation axis and, for each condition, 1000 PMT traces were recorded. Figure 17 presents the integrated N$_2$ signals recorded with the PMT based LIDAR as a function of the turbulence position. The filamentation zone is indicated with the blue square on the right hand side of Figure 17. As expected, the recorded signal increases as the turbulence zone comes closer to the filamentation. This behavior is similar to what has been previously observed by the *Teramobile* group [21].
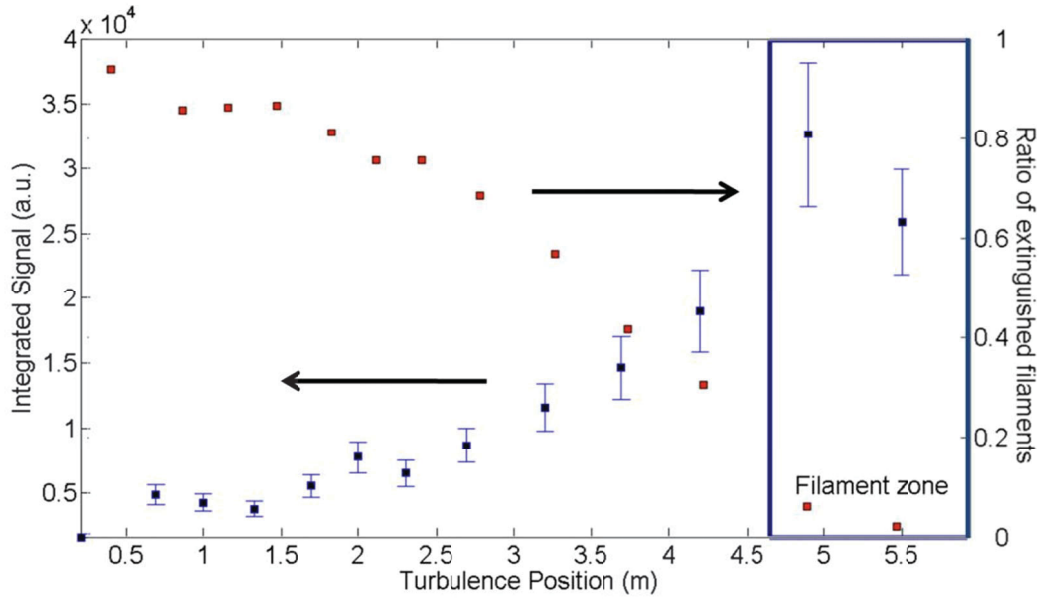
Figure 17: Longitudinal integration of the backscattered signals collected with the LIDAR system

However, it is clear that, even though the filaments survive the interaction with the strong turbulence zone, the collected fluorescence signal, at around 3.25×10^4 a.u., is significantly lower than that observed when no turbulence was inserted in the beam path (integration$_{no\ Turb}$ = 9.7×10^4 a.u., not shown on the figure). The filamentation survival is confirmed by the filament extinction curve. For each laser shot, the fluorescence signal is integrated and compared to the integral of the background (0 m to 4 m). If the integrated signal is higher than the background integral plus three times its standard deviation, the filaments are considered as having survived the interaction with the turbulence source; otherwise, they are considered as extinct. From this curve, we notice that as the turbulence source comes closer to the signal zone, the probability of filaments' extinction decreases and comes close to zero when the turbulence source is inserted in the plasma column.

Figure 18 provides a hint of the physical mechanisms involved during the interaction with a strong and localized turbulence zone.

36

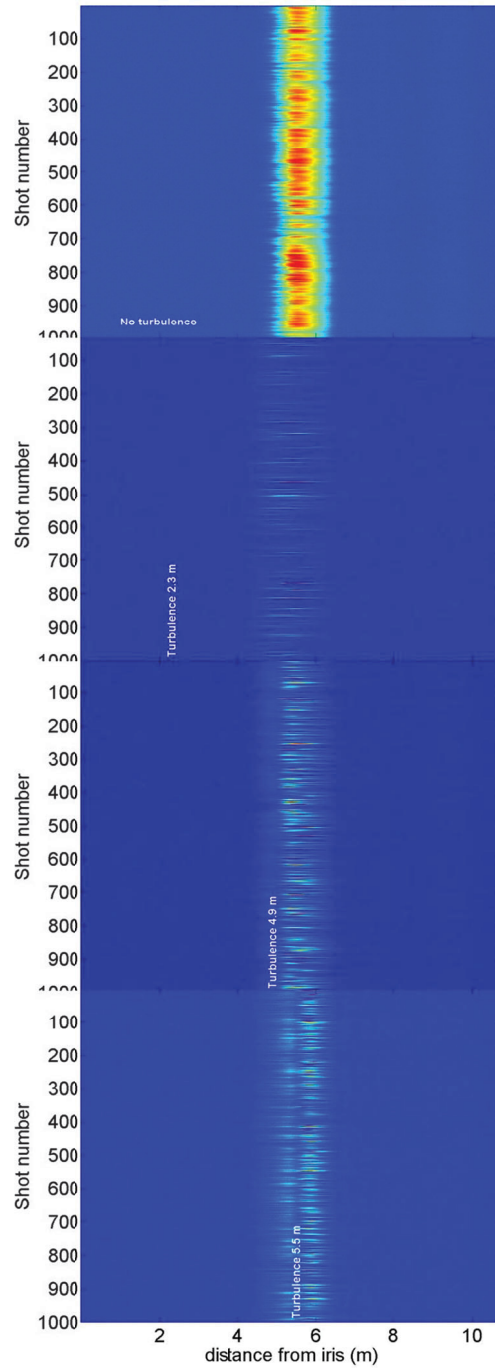*Figure 18: Backscattered signals recorded with a PMT based LIDAR*

a) (top) unperturbed medium, b) turbulence 2.3 m after the aperture, c) turbulence 4.9 m after the aperture and d) (bottom) 5.5 m after the aperture. The horizontal axis corresponds to the distance from the aperture, the vertical scale is the shot number and the color scale corresponds to the signal intensity.

For Figures 18 a-d (a-d is from top downwards), the horizontal axis corresponds to the propagation distance from the aperture, the vertical axis corresponds to the number of the individual shot and the color scale corresponds to the collected signal intensity in arbitrary units. Each individual trace corresponds to the N_2 signal produced with a single laser shot. Figure 18a presents the situation when no turbulence was inserted in the beam propagation axis. The fluorescence signal collected is rather stable from shot-to-shot both in intensity and in position. As expected, when the turbulence is inserted between the aperture and the filamentation zone (Figure 18b, turbulence position 2.3 m), the fluorescence signal recorded by the detector is on average 14 times weaker and rather unstable in both intensity and localization. Figure 18c and 18d present the results when the heat gun is inserted in the filamentation zone. It can be seen that the hot air turbulent zone significantly reduces the produced fluorescence intensity. Moreover, when it is inserted in the center of the filament zone (Figure 18d), the fluorescence signal is partially extinguished in the turbulence zone and immediately after, returns to its normal level. As discussed in the following section, this local extinction is not attributed to an increase in C_n^2, but rather to the N_2 temperature dependent fluorescence yield.

3.3   Discussion

The fluorescence signal extinction observed when the hot air turbulent zone is inserted in the filaments' zone is due both to a reduction of the filament intensity in this area and a decrease of the fluorescence yield in the hot air stream. For the first case, the decrease of the filament intensity has been well described by the simulations performed by Ma *et al.*[31]. In fact, they observed that the filaments' diameters were widened to mm size when propagating in a turbulent medium. This widening effect caused a significant reduction of the filament intensity to 10^{12} W/cm^2, just above the ionization threshold for air. They explained that this widening effect is caused by a distortion of the pulse's background reservoir which cannot efficiently replenish the filaments' core anymore. This effect explains the overall decrease by a factor of three for the integrated fluorescence signal in Figure 17 when the turbulence was inside the filamentation zone. Actually, as discussed in the experimental setup, even though the turbulent stream of hot air is considered punctual (2 cm), its presence along the beam path increased the neighboring value of C_n^2 in a 1 m radius around the turbulence source. The lengthening of the filaments in Figure 18c - 18d originates from random intensity modulations of the energy reservoir induced by the turbulence which form multiple filaments at different distances.

The effect of the localized hot air turbulent zone on the fluorescence yield is presented in Figure 19 in which the 1000 backscattered traces shown in Figure 18d (turbulence position 5.5 m after the aperture) have been summed.
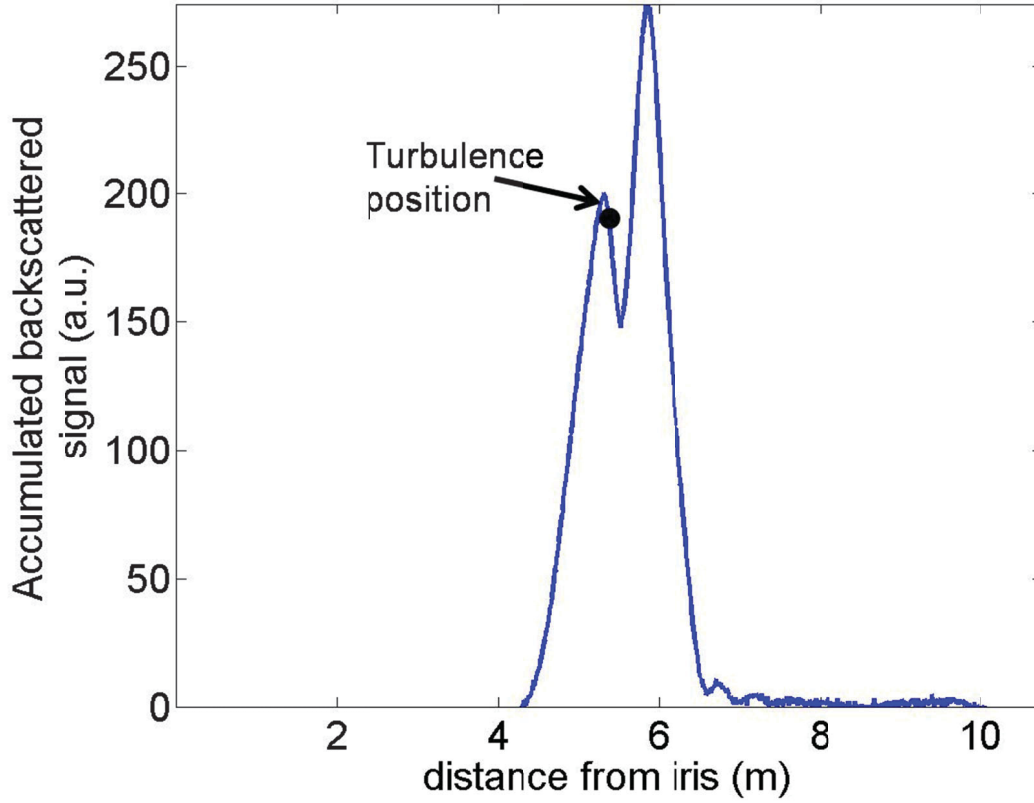
Figure 19: Sum of the 1000 curves from figure 18d. The black dot corresponds to the position of the turbulence medium

The position of the turbulence zone is indicated by the black dot on the curve. The sharp dip observed in Figure 19 is attributed to the decrease of the nitrogen fluorescence yield in the 600ºC environment generated by the heat gun. An increase of the air temperature from 20 ºC to 600 ºC would decrease the nitrogen fluorescence yield in the wave band between 300 nm and 406 nm [39, 40]. Indeed, based on an experiment performed with an electron beam, it was found that the fluorescence yield (ξ) of N_2 between 300 nm to 406 nm is proportional to:

$$\epsilon \sim \rho \left(\frac{A_1}{1 + \rho B_1 \sqrt{T}} + \frac{A_2}{1 + \rho B_2 \sqrt{T}} \right) \tag{7}$$

where ρ is the air density at the prescribed pressure and temperature, T is the temperature (K) and $A_1 = 147.4$ m^2kg^{-1}, $A_2 = 69.8$ m^2kg^{-1}, $B_1 = 2.4$ $m^3kg^{-1}K^{-1/2}$, $B_2 = 20.1$ $m^3kg^{-1}K^{-1/2}$ are constants determined experimentally [33]. The two terms presented in the equation describe the fluorescence yield of the 2P lines and the 1N line. Based on this approximation, we found that the fluorescence yield decreases by 60 % when the temperature passes from 293 K to 873 K and is in good agreement with the measurement where the signal locally decreased by 52 %.

Even though the heat gun's stream of air was only 2 cm large, the limited response time of the PMT (1-2ns) broadened the apparent width of this dip. The position of the

turbulence zone was also localized approximately 20 cm before the observed dip. This spatial shift is simply caused by the fluorescence lifetime of the N_2 molecule which is approximately 1-2 ns. This behavior would delay the dip position approximately 30 cm to 60 cm after the turbulence zone.

3.4   Conclusion

In this part of the research, the effects of a strong and localized turbulence on laser filamentation were studied using a PMT based LIDAR to directly observe and characterize, via N_2 molecular fluorescence, the filaments' plasma distribution. The filaments' elimination when the turbulent zone was placed prior to filamentation was confirmed. However, when the hot turbulent source was inserted in the plasma zone, a clear reduction of the filaments' emissions was observed, though not a total extinction of them. The overall decrease of the fluorescence is explained by an increased diameter of the filament core due to the induced distortion of the background reservoir which leads to a reduction of the filaments' intensity. The sharp dip was caused by a localized decrease of the nitrogen fluorescence yield in the hot stream of air.

This interesting behavior of filaments in hot air turbulent medium could lead to multiple interesting atmospheric applications. One of them consists in the detection of aircrafts which cannot be detected with conventional radars. In fact, the air turbulence induced by their jet engines could be detected and positioned using the method described, giving the exact position of the aircraft. This method could not be used for global positioning of aircrafts but could be used in specific areas where secrecy and security is of major importance.

4 AO SYSTEM FOR COMPENSATION OF ATMOSPHERIC TURBULENCES

Atmospheric turbulence is a great challenge for remote applications of filamentation. In fact, multiple experiments, including the ones reported here, demonstrated that if a source of turbulence is inserted in the beam path before the filaments, the formation of plasma will be rather weak and suffer from shot-to-shot fluctuations. The AO system presented in this document could potentially solve this problem by altering the initial wavefront such that the transverse phase shifts associated to the propagation in the turbulent medium are compensated at the time the filaments form. To test this idea, a source of turbulence (infrared lamp, $C_n^2 \approx 5 \times 10^{-12}$ m$^{-2/3}$) is inserted immediately after the telescope output, between the DM and the WFS. As a consequence, the wavefront modifications caused by the propagation in turbulent air can be measured by the WFS and, hopefully, be pre-compensated for by the DM. Here again, the filaments are characterized by the N_2 fluorescence emitted by the plasma left behind the laser pulse using a PMT-based LIDAR. Three conditions were tested,

1) No turbulence with AO system compensation, 2) Turbulence without AO system compensation, 3) Turbulence with AO system compensation

and the results are presented in Figure 20. Note that for condition 2, the wavefront aberrations of the initial pulse are pre-compensated with an offset voltage applied on some of DM's actuators. The plots show that even though the AO system cannot totally compensate the wavefront alterations produced by the propagation through the turbulent medium, the N_2 peak signal is increased by a factor of 2.3 when the AO system is working (condition 3).
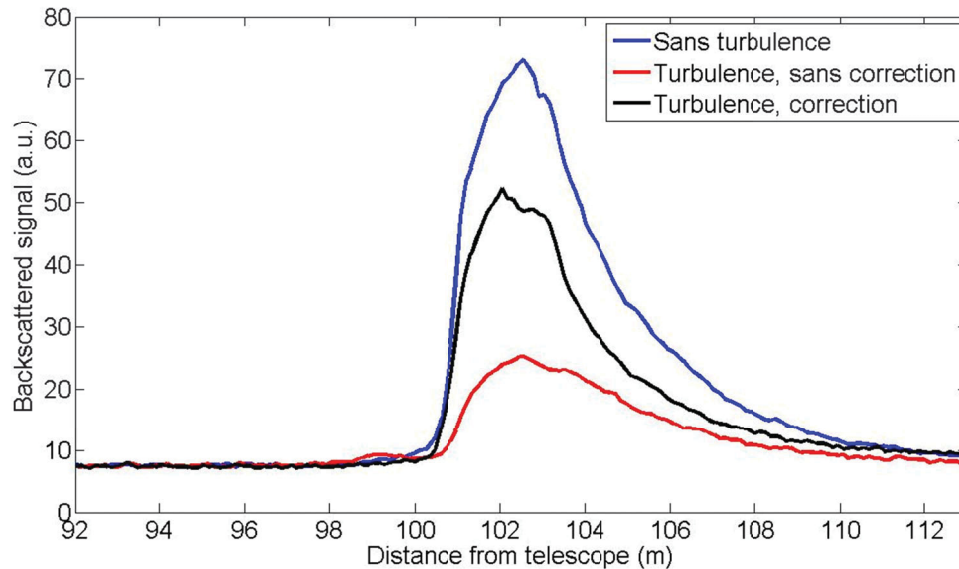

Figure 20: Plasma distribution of laser filaments produced at a long distance. Three conditions are presented: blue) Without turbulence; red) turbulence, no AO compensation; black) Turbulence, with AO compensation

This page intentionally left blank.

References

[1] A. Braun, G. Korn, X. Liu, D. Du, J. Squier, and G. Mourou, "Self-channeling of high-peak-power femtosecond laser pulses in air," Opt. Lett. **20**, 73- (1995)

[2] S.L. Chin, S.A. Hosseini, W. Liu, Q. Luo, F. Théberge, N. Akozbek, A. Becker, V.P. Kandidov, O.G. Kosareva, and H. Schroeder, The propagation of powerful femtosecond laser pulses in optical media: physics, applications, and new challenges, Canadian Journal of Physics, **83**, 863-905 (2005)

[3] L. Wöste, C. Wedekind, H. Wille, P. Rairoux, B. Stein, S. Nikolov, Ch. Werner, S. Niedermeier, H. Schillinger, and R. Sauerbrey, "Femtosecond atmospheric lamp," Laser Optoelektron. 29, 51-53 (1997)

[4] M. Mlejnek, E. M. Wright, and J. V. Moloney, "Dynamic spatial replenishment of femtosecond pulses propagating in air," Opt. Lett. **23**, 382-384 (1998)

[5] A. Couairon and A. Mysyrowicz, "Femtosecond filamentation in transparent media", Phys. Rep. 441 (2007) 47

[6] J.-F. Daigle, P. Mathieu, G. Roy, J.-R. Simard, S.L. Chin, Multi-constituents detection in contaminated aerosol clouds using remote-filament-induced breakdown spectroscopy, Optics Communications, 278, 147, (2007)

[7] G. Méjean, J. Kasparian, E. Salmon, J. Yu, J-P Wolf, R. Bourayou, R. Sauerbrey, M. Rodriguez, L. Wöste, H. Lehmann, B. Stecklum, U. Laux, J. Eislöffel, A. Scholz, A. P. Hatzes, Towards a supercontinuum-based infrared lidar, Appl. Phys. B 77, 357–359 (2003)

[8] Q. Luo, H.L. Xu, S.A. Hosseini, J.-F. Daigle, F. Theberge, M. Sharifi, S.L. Chin, Remote sensing of pollutants using femtosecond laser pulse fluorescence spectroscopy, Applied Physics B, 82, 105-109 (2006)

[9] S. Tzortzakis, B. Prade, M. Franco, A. Mysyrowicz, S. Hüller, and P. Mora, Femtosecond laser-guided electric discharge in air, Phys. Rev. E 64, 057401 (2001)

[10] N. Goto, M. Miki, T. Fujii, T. Nayuki, T. Sekika, T. Shindo, K. Nemoto, Electrical Discharge Induced by Ultra-Short High-Power Laser-Triggering and Guiding Effect, Transactions of the Institute of Electrical Engineers of Japan. A, 125, 12,1059-1064 (2005)

[11] R. M. Measures. *Laser Remote Sensing: Fundamentals and Applications*. Krieger Publishing Company, Florida, first edition, 1992

[12] S. L. Chin, H. Xu, Q. Luo, F. Théberge, W. Liu, J.-F. Daigle, Y. Kamali, P. T. Simard, J. Bernhardt, S. A. Hosseini, M. Sharifi, G. Méjean, A. Azarm, C. Marceau, O. Kosareva, V. P. Kandidov, N. Aközbek, A. Becker, G. Roy, P. Mathieu, J.-R. Simard, M. Châteauneuf, and J. Dubois. Filamentation remote sensing of chemical and biological agents/pollutants using only one femtosecond laser source. *Applied Physics B: Lasers and Optics*, 95:1–12, 2009. 10.1007/s00340-009-3381-7

[13] Ph. Rohwetter, K. Stelmaszczyk, L.Wöste, R. Ackermann, G. Méjean, E. Salmon, J. Kasparian, J. Yu, and J.-P. Wolf. Filament-induced remote surface ablation for long range laser-induced breakdown spectroscopy operation. *Spectrochimica Acta Part B: Atomic Spectroscopy*, 60(7-8):1025 – 1033, 2005

[14] F.A. Theopold, J-P. Wolf, L. Wöste, DIAL Revisited : BELINDA and white-light femtosecond Lidar, *in* C. Weitkamp, Lidar : Range-resolved optical remote sensing of the atmosphere, Springer, 2005, 399-443

[15] J. Kasparian, J-P. Wolf, Physics and applications of atmospheric nonlinear optics and filamentation, Opt. Express, 16, 466-493 (2008)

[16] Kasparian, R. Sauerbrey, and S. L. Chin, The critical laser intensity of self-guided light filaments in air, Appl. Phys. B: Lasers Opt. 71, 877 (2000)

[17] A Becker, N. Akozbek, K. Vijayalakshmi, E. Oral, C.M. Bowden, S.L.Chin, Intensity clamping and re-focusing of intense femtosecond laser pulses in nitrogen molecular gas, Applied Physics B, 73, 287-290 (2001)

[18] R.Ackermann, G. Méjean, J. Kasparian, J. Yu, E. Salmon and J.-P. Wolf. Laser filaments generated and transmitted in highly turbulent air. *Optics Letters,* Vol. 31, 1, p. 86 (2006)

[19] A.M. Weiner, Femtosecond pulse shaping using spatial light modulators, Rev. Sci. Instrum., **71**, **5**, 1929 (2000)

[20] M. Rodriguez, R. Bourayou, G. Méjean, J. Kasparian, J. Yu, E. Salmon, A. Scholz, B. Stecklum, J. Eislöffel, U. Laux, A.P. Hatzes, R. Sauerbrey, L. Wöste and J-P. Wolf, Kilometer-range nonlinear propagation of femtosecond laser pulses, Phys. Rev. E, **69**, 036607-1 (2004)

[21] Z. Jin, J. Zhang, M.H. Xu, X. Lu, Y.T. Li, Z.H. Wang and Z.Y. Wei, Control of filamentation induced by femtosecond laser pulses propagating in air, Opt. Express, **13**, **25**, 10424 (2005)

[22] W. Liu, F. Theberge, J.-F. Daigle, P.T. Simard, S.M. Sarifi, Y. Kamali, H.L. Xu, S.L. Chin, An efficient control of ultrashort laser filament location in air for the purpose of remote sensing, Applied Physics B, **85, 1**, 55 (2006)

[23] S. Eisenmann, E. Louzon, Y. Katzir, T. Palchan, A. Zigler, Y. Sivan and G. Fibich, Control of the filamentation distance and pattern in long-range atmospheric propagation, Op.t. Express, **15**, **6**, 2779 (2007)

[24] J.-F. Daigle, G. Mejean, W. Liu, F. Theberge, H.L. Xu, Y. Kamali, J. Bernhardt,
A. Azarm, Q. Sun, P. Mathieu, G. Roy, J.-R. Simard, and S. L. Chin. Long
range trace detection in aqueous aerosol using remote filament-induced break-
down spectroscopy. *Applied Physics B: Lasers and Optics*, 87:749–754,
2007.10.1007/s00340-007-2642-6

[25] C. Favre, V. Boutou, S. C. Hill., W. Zimmer, M. Krenz, H. Lambrecht, J. Yu, R. K. Chang, L. Wöste, and J.-P. Wolf. White-light nanosource with directional emission. *Phys. Rev. Lett.*, 89(3):035002, 2002

[26] R.Ackermann, G. Méjean, J. Kasparian, J. Yu, E. Salmon and J.-P. Wolf. Laser filaments generated and transmitted in highly turbulent air. *Optics Letters,* Vol. 31, 1, p. 86 (2006)

[27] R. Salamé, Né Lascoux, E. Salmon, R. Ackermann, J. Kasparian and J.-P. Wolf. Propagation of laser filaments through an extended turbulent region. *Applied Physics Letters*, 91, p. 171106 (2007)

[28] A. Houard, M. Franco, B. Prade, A. Durécu, L. Lombard, P. Bourdon, O. Vasseur, B. Fleury, C. Robert, V. Michau, A. Couairon and A. Mysyrowicz. Femtosecond filamentation in turbulent air. *Physical Review A*, 78, p. 033804 (2008)

[29] J.R. Penano, P. Sprangle, B. Hazafi, A. Ting, D.F. Gordon and C.A. Kapetanakos. Propagation of ultra-short, intense laser pulses in air. *Physics Plasmas*, 11, p. 2865 (2004)

[30] V.P. Kandidov, O.G. Kosareva, M.P. Tamarov, A. Brodeur & S.L. Chin. Nucleation and random movement of filaments in the propagation of high-power laser radiation in a turbulent atmosphere. *Quantum Electronics*, 29, pp. 911-915 (2009)

[31] Y. Ma, X. Lu, T. Xi, Q. Gong and J. Zhang. Widening of long-range femtosecond laser filaments in turbulent air. *Optics express*, Vol. 16, 12, p. 8332 (2008)

[32] G. Méjean, A. Couairon, Y.-B. André, C. D. Amico,M. Franco, B. Prade, S. Tzortzakis, A. Mysyrowicz and R. Sauerbrey. Long range self-channelling of infrared laser pulses in air: a new propagation regime without ionization. *Applied Physics B*, 79, p. 379 (2004)

[33] J.-F. Daigle, O. Kosareva, N. Panov, M. Bégin, F. Lessard, C. Marceau, Y. Kamali, G. Roy, V.P. Kandidov, and S.L. Chin. A simple method to significantly increase filaments' length and ionization density. *Appl. Phys. B*, 94, p. 249 [2009]

[34] Measures, R. M. *Laser Remote Sensing: Fundamentals and Applications.* Florida : Krieger, ISBN 0-89464-619-2 (2002)

[35] Schott UG11 transmission data sheet. *Optical-Filters.com.* [Online] 2009. http://www.optical-filters.com/ug11.html

[36] A. Iwasaki, N. Aközbek, B. Ferland, Q. Luo, G. Roy, C.M. Bowden and S. L. Chin. A LIDAR technique to measure the filament length generated by a high-peak power femtosecond laser pulse in air. *Applied Physics B*, 76, p. 231 (2003)

[37] Clifford, S.F. Temporal-Frequency spectra for a spherical wave propagating through turbulent atmosphere. *Journal of the Optical Society of America*, Vol. 61, 10, p. 1284 (1971)

[38] M. Nagano, K. Kobayakawa, N. Sakaki and K. Ando. New measurement on photon yields from air and the application to the energy estimation of primary cosmic rays. *Astroparticle Physics*, Vol. 22, 3-4, p. 235 (2004)

[39] F., Arciprete et al. AIRFLY : Measurement of the fluorescence yield in the atmospheric gases. *29th International Cosmic Ray Conference Pune*, pp. 101-106 (2005)

This page intentionally left blank.

DOCUMENT CONTROL DATA

(Security classification of title, body of abstract and indexing annotation must be entered when the overall document is classified.)

1. ORIGINATOR (Name and address of the organization preparing the document.) Robert Bernier Les instrument optique du St-Laurent 17500 Montée Gascon Mirabel, Québec, J7J 2C5	2. SECURITY CLASSIFICATION (Overall security classification of the document, including special warning terms if applicable.) UNCLASSIFIED (NON-CONTROLLED GOODS DMC A REVIEW: GCEC JUNE 2010

3. TITLE (The complete document title as indicated on the title page. Its classification should be indicated by the appropriate abbreviation (S, C or U) in parentheses after the title.)

    Adaptive optics system for remote sensing applications of filamentation

4. AUTHORS (Last name, followed by initials – ranks, titles, etc. not to be used.)

    Jean Francois Daigle and Robert Bernier

5. DATE OF PUBLICATION (month and year of publication of document.) March2011	6. NO. OF PAGES (Including Annexes, Appendices and DCD sheet.) 51

7. DESCRIPTIVE NOTES (the category of the document, e.g. technical report, technical note or memorandum. If appropriate, enter the type of report, e.g. interim, progress, summary, annual or final. Give the inclusive dates when a specific reporting period is covered.)

    Contractor Report

8a. PROJECT OR GRANT NO. (If appropriate, the applicable research and development project or grant number under which the document was written. Please specify whether project or grant)	8b. CONTRACT NO. (If appropriate, the applicable number under which the document was written) W7701-071506
9a. ORIGINATOR'S DOCUMENT NUMBER (Official document number by which the document is identified by the originating activity. Number must be unique to this document.) DRDC Valcartier CR 2011-539	9b. OTHER DOCUMENT NOS. (Any other numbers which may be assigned to this document either by the originator or the sponsor.)

10. DOCUMENT AVAILABILITY (Any limitation on further distribution of the document, other than those imposed by security classification.)

    (x) Unlimited distribution
    ( ) Distribution limited to defence departments
    ( ) Distribution limited to defence contractors
    ( ) Distribution limited to government
    ( ) Distribution limited to Defence R&D Canada
    ( ) Controlled by Source

11. DOCUMENT ANNOUNCEMENT (Any limitation to the bibliographic announcement of this document. This will normally correspond to the Document Availability (10). However, where further distribution (beyond the audience specified in (10) is possible, a wider announcement audience may be selected.)

    Unlimited

UNCLASSIFIED
SECURITY CLASSIFICATION OF FORM

12. ABSTRACT   (Brief and factual summary of the document. May also appear elsewhere in the body of the document itself. It is highly desirable that the abstract of classified documents be unclassified.   Each paragraph of the abstract shall begin with an indication of the security classification of the information in the paragraph (unless the document itself is unclassified) represented as (S), (C), or (U). May be in English only).

Laser filaments represent a potentially useful tool in terms of remote and atmospheric applications. Indeed, the high intensity inside the filament core induces nonlinear effects which can broaden the spectrum from the ultraviolet to the mid-infrared. This white light laser could be used as an effective counter measure to blind detectors or guide missiles away from the target. Moreover, its intensity is sufficiently high to ionize the transparent medium in which it propagates. The ionized atoms and molecules recombine and emit a fingerprint fluorescence, characteristic of the ionized element. This property of filamentation opens the way for remote sensing applications. However, the generation and control of those filaments poses real challenges. This report is about the work that has been done at RDDC-Valcartier, in collaboartion with Laval University, to design, develop and test an adaptive optics (AO) system to be used with a lidar in remote sensing applications. This AO system has been tested to allow initiation of filaments as far as 120 m from the lidar laser source. Also, in this work, the influence of atmospheric turbulences on the initiation and strength of the filamentation process has been studied.

13. KEYWORDS, DESCRIPTORS or IDENTIFIERS (Technically meaningful terms or short phrases characterizing a document and could be helpful in cataloguing it. Should be **Unclassified** text. If not , the classification of each term should be indicated as with the title. Equipment model designation, trade name, military project code name, and geographic location may be included. If possible, should be selected from a published thesaurus. e.g. Thesaurus of Engineering and Scientific Terms (TEST) and that thesaurus-identified.)

Supercontinuum lidar, remote sensing, contaminants, filamentation, turbulences, adaptive optics

UNCLASSIFIED
SECURITY CLASSIFICATION OF FORM

Defence R&D Canada

Canada's Leader in Defence
and National Security
Science and Technology

R & D pour la défense Canada

Chef de file au Canada en matière
De science et de technologie pour
la défense et la sécurité nationale

DEFENCE **R&D** DÉFENSE

www.drdc-rddc.gc.ca